Scientific Research Publishing

World Journal of Mechanics, 2025, 15(8), 135-167
https://www.scirp.org/journal/wjm
ISSN Online: 2160-0503
ISSN Print: 2160-049X

Torque-Angle Tightening: New Theoretical and Practical Approach

Zouhair Chaib, Christophe Delcher

Assemblies Department, Technical Center for Mechanical Industries (CETIM), Senlis, France
Email: Zouhair.Chaib@Cetim.fr, Christophe.Delcher@cetim.fr

How to cite this paper: Chaib, Z. and Delcher, C. (2025) Torque-Angle Tightening: New Theoretical and Practical Approach. *World Journal of Mechanics*, **15**, 135-167.
https://doi.org/10.4236/wjm.2025.158008

Received: August 1, 2025
Accepted: August 28, 2025
Published: August 31, 2025

Abstract

Static and dynamic capacities of bolted connections are highly dependent on the preload. For this reason, and due to the inaccuracy of torque tightening technology, many other tightening technologies and preload monitoring have been developed. This paper discusses the concept, the theoretical and the practical approach of the combined tightening method called "Torque-Angle Tightening". It's an old tightening technology that consists of a first step to apply a snug torque, then to apply a required angle in a second step. It allows for a more accurate preload compared to the torque tightening. VDI2230 gives some values of the tightening factors for many tightening technologies. This paper provides some new formulas that reduce the error level (difference) between the calculated and real introduced preloads in the bolts. It details some best practices to evaluate the required parameters and to apply the tightening operation correctly. Experimental tests and FE analysis are used to evaluate this improvement of the existing formula.

Keywords

Torque-Angle, Combined Tightening, Bolt Preload, Snug Torque, Elasto-Plastic Tightening

1. Introduction

Bolting connections are used in all mechanical structures or substructures for different reasons. For critical and structural applications, the bolt's preload must be correctly introduced to ensure good joint behaviors and to prevent all risks of sliding (micro or macro sliding), contact opening or parting line separation and in other cases to compensate for any preload loosening (thermal loading, creeping, yielding, …) [1]-[3].

Due to the deviations of friction factors, tightening tools and other parameters,

the preload is defined by three levels: the nominal level, which is currently used for simplified analysis and the minimum and the maximum levels, which are used for critical analysis. Some references [1] [2] use the tightening factor given by equation (1) to compare the accuracy of all tightening techniques. By using this factor and the table of the VDI 2230 [1], the Torque-Angle tightening is more accurate than the torque tightening. But there is no accurate formula that can be used by designers to define the snug torque and the required angle to achieve the target preload and its accuracy. For steel construction (HR and HV bolts), some simplified tables are provided in the European standard EN 1090-2 [4]. Other simplified formulas are given by Cetim [5], Guillot [6], Alkatan [7], Massol [8] and Bickford [9].

$$\alpha = \frac{\text{Maximal level of introduced load}}{\text{Minimal level of introduced load}} \tag{1}$$

Fukuoka [10] gives an advanced calculation of the relation between the applied angle and the preload. According to his papers, the gap between the theoretical calculations and the real introduced preload is mainly due to the settlement that occurs in contact surfaces and geometrical clearance. But according to Gold [11], this gap is due to the elastic assumption used to calculate the resilience (stiffness) of clamped parts and bolts.

To overcome this limitation, two main solutions have been advanced. The first one, used by some industrial companies, consists of performing experimental tests to qualify the optimal snug torque and the total angle to be applied. The second solution consists of performing a tightening up to the yield point (stopping tightening if the torque-angle gradient is down [1]) or over the yield point as developed by Friedrich [12], Chavan [13] and Göran [14]. This solution is commonly used in steel construction and for some automotive applications. Baghua [15] had studied the effect of the snug level on the final preload accuracy. Deepa [16] and Eccles [17] had treated and compared the torque to the combined tightening throw experimental tests.

The yielding tightening offers accurate preload with no equivalent or higher service performance than tightening in the elastic area (70% to 90% YLS) according to fatigue tests made by Kraemer [18].

2. Basic Knowledge about the Combined Tightening

2.1. Measurement of Friction Coefficients in Bolted Connection

The measurement of friction coefficients according to ISO 16047 [19] consists of using a specific test-bench defined by a controlled engine and 6 axis load-cell. After installing a specimen that represents the real assembly, one side of specimen will be locked (the nut, or the bolt head in our case). Then, a regular tightening rotation angle is applied to the second side. The used load-cell measures, the total applied torque "T", the bearing surface torque of the turned side "T_b", the thread torque "T_{th}" (useful torque + friction torque due to the movement between the screw thread and its nut thread), the clamped load "F_0", the applied angle "θ" and

the tightening time.

Measured torques are defined by equations given below:

- Bearing surface torque: $T_b = F_0 \times \mu_b \times \frac{D_b}{2}$ where "D_b" is the mean bearing diameter of the turned side. It is done by the medium value of inner and outer diameters of contact surface situated between the turned side and the clamped part.
- Thread torque: $T_{th} = F_0\left(\frac{P}{2\pi} + 0,577 \times d_2 \times \mu_t\right)$ including the useful torque $T_u = F_0 \times \frac{P}{2\pi}$.
- Total torque:

$$T = T_b + T_{th} = F_0\left(\frac{P}{2\pi} + 0.577 \times d_2 \times \mu_t + \frac{D_b}{2} \times \mu_b\right) \quad (2)$$

where, P: thread Pitch.

d_2: pitch diameter of the bolt thread: $d_2 = d - 0.6495 \times P$.

d: nominal thread diameter of the bolt.

For each measured point, friction coefficients could be obtained by using equations below:

- Bearing surface friction coefficient: $\mu_b = \frac{T_b}{F_0 \times \frac{D_b}{2}}$.
- Thread friction coefficient: $\mu_t = \frac{\frac{T_{th}}{F_0} - \frac{P}{2\pi}}{0.577 \times d_2}$.

Default values used for a non-qualified case is 0.15 ± 0.03 (e.g. Zinc Flake coating).

2.2. Definition of the Snug Torque

During tightening, the measured Torque-Clamp Force graph commonly shows a linear relationship between these factors. But the torque-angle graph shows three main areas:

1) A first non-linear area at the beginning of tightening. In fact, due to geometric defects and roughness, the contact between the parts at this stage is not perfect and not stable. At the moment, no analytical formula or numerical approach can be industrially used to determine this area. The end of this area defines the minimum level of the snug torque.

2) A second linear area shows a linear relationship between Torque-Angle and between Angle-Preload. This area can be represented by an analytical formula detailed in the paragraphs below. Most of the time, designers prefer to work in this area to prevent the assembly exceeding the yield point.

3) A third non-linear area, highly defined by clamped length, bolt design and their material properties (YLS, ULS, A%,…).

As mentioned above, for the snug torque, the designers and operators ignore

the first non-linear area. For elastic tightening, this snug torque can be estimated by the torque that introduces a preload close to 30% of the final preload. And for a tightening at or after the yield point, this ratio can achieve 50% ([1], [3] and [12]).

By using the standard ISO 16047 [19], friction values, geometric data of assembly and tightening tool accuracy, the snug torque could be calculated by using Equation (2) as:

$$T_{snug} = F_{snug}\left(\frac{P}{2\pi} + 0.577 \times d_2 \times \mu_t + \frac{D_b}{2} \times \mu_b\right) \tag{2-b}$$

where: F_{snug} : introduced preload by applying the snug torque.

2.3. Calculation of Required Angle

To calculate the required angle to introduce a target preload, the bolt and clamped parts can be represented by two elastic springs, which can be easily calculated using the listed references [1]-[9] or other equivalent references. Applying any additional preload "ΔF_0" will elongate the bolt and will compress clamped parts respectively by "ΔL_b" and "ΔL_P" given by Equation (3) and Equation (4). And due to the helicoidal shape of the threads, the relative rotation of the nut with respect to the screw "$\Delta\theta$" will create a relative displacement of the nut "ΔL_{sn}", calculated by two ways, Equation (5) and Equation (6). Finally, the relationship between the preload and the applied angle is detailed by Equation (7), which illustrates the importance of the thread pitch, the bolt resilience (stiffness), and the clamped parts in addition to the applied angle to calculate the preload. This formula is used in most academic and industrial applications.

$$\Delta L_b = \frac{F_0}{K_b} = F_0 \times \delta_b \tag{3}$$

$$\Delta L_P = \frac{F_0}{K_P} = F_0 \times \delta_P \tag{4}$$

$$\Delta L_{sn} = \frac{P}{360}\Delta\theta \tag{5}$$

$$\Delta L_{sn} = \Delta L_b + \Delta L_P \tag{6}$$

$$\Delta F_0 = \frac{P}{360 \times \left(\delta_b + \delta_p\right)}\Delta\theta \tag{7}$$

$$F_0 = \frac{T_{sung}}{\frac{P}{2\pi} + 0.577 \times d_2 \times \mu_t + \frac{D_b}{2} \times \mu_b + \frac{\Delta\theta}{\frac{360 \times \left(\delta_b + \delta_p\right)}{P} + \left(\frac{P}{2\pi} + 0.577 \times d_2 \times \mu_t\right) \times \delta_{b,t}}} \tag{8}$$

where: F_0 : Bolt Preload.

δ_b and δ_P : Axial resilience (stiffness) of bolt and clamped parts.

$\delta_{b,t}$: Torsion resilience (stiffness) of bolt.

For very long clamping length, the bolt torsion angle can be significant. For this reason, we (Cetim) have improved the last formula as shown by Equation (8).

3. Experimental and Critical Analysis of Existing Formulas

Because of the negative feedback from French manufacturers to define the appropriate angle and snug torque without experimental qualification, we have performed experimental tests to evaluate the existing formula and gain a better understanding of this tightening technique.

3.1. Experimental Program

This program covers 37 assembly configurations. These configurations were defined with a group of French manufacturers (~60 companies). Figure 1 and Table 1 give a simplified view of the tested assembly configurations. Each tested assembly is defined by a screw or a stud (#1), a nut or a tapped part (#2), 0 to 2 washers (#3) that depend on the tested configuration, a set of clamped parts (#4) and a load sensor (#5) to measure the load in the bolt.

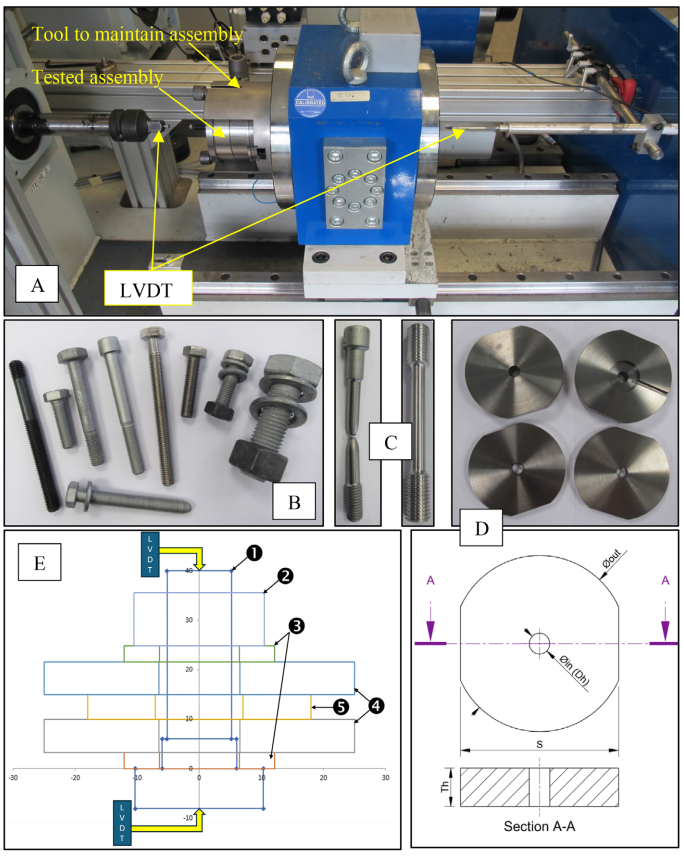

A: Torque-Tension test-bench; B: Tested fasteners; C: specimen used in tensile test; D: Clamped parts and E: illustration of tested configuration where: 1-Screw, 2-Nut, 3-Washer, 4-Clamped parts, 5-Load sensor.

Figure 1. Overview of tested assembly and components.

Table 1. (a): Details of experimental program. (b): Geometric and material data of clamped parts.

(a)

Config ID	Lk/d	Screw or Stud	Washer or Nut	Part 1	Part 2	Part 3	Part 4	Part 5	Part 6	Part 7
CONF_01	2	Screw HR 10.9 - M12x40	Washer HR M12	E1 - S235 J2-1D	CLP 80 KN	E2-S235J2-1D	Washer HR M12	Nut HR M12 10.9		
CONF_02	6	Screw HR 10.9 - M12x80	Washer HR M12	E3-S235J2-1D	E4-42CD4 - 2D	CLP 80 KN	E5-42CD4 - 2D	E6-42CD4 - Cale	Washer HR M12	Nut HR M12 10.9
CONF_03	2	Screw HV 10.9 - M12-40/25 PGB	Washer HV M12	E1 - S235 J2-1D	CLP 80 KN	E2-S235J2-1D	Washer HV M12	Nut HV M12 10.9 PGB		
CONF_03B	2	Screw HV 10.9 - M12-40/25 PEINER	Washer HV M12	E1 - S235 J2-1D	CLP 80 KN	E2-S235J2-1D	Washer HV M12	Nut HV M12 10.9 PEINER		
CONF_04	6	Screw HV 10.9 - M12-80/40 PGB	Washer HV M12	E3-S235J2-1D	E4-42CD4 - 2D	CLP 80 KN	E5-42CD4 - 2D	E6-42CD4 - Cale	Washer HV M12	Nut HV M12 10.9 PGB
CONF_04B	6	Screw HV 10.9 - M12-80/40 PEINER	Washer HV M12	E3-S235J2-1D	E4-42CD4 - 2D	CLP 80 KN	E5-42CD4 - 2D	E7-S235 J2 - 1D	Washer HV M12	Nut HV M12 10.9 PEINER
CONF_05	2	Screw HR 10.9 - M24-80	Washer HR M24	E28-M24-S235-2D	Washer HR M24	Nut HR M24 10.9				
CONF_06	6	Screw HR 10.9 - M24-130/70	Washer HR M24	E29-M24-S235-5D	Washer HR M24	Nut HR M24 10.9				
CONF_07	2	Screw HV 10.9 - M24-80/45	Washer HV M24	E28-M24-S235-2D	Washer HV M24	Nut HV M24 10.9				
CONF_08	6	Screw HV 10.9 - M24-130/43	Washer HV M24	E28-M24-S235-2D	E28-M24-S235-2D	E33-M24-S235-cale	Washer HV M24	Nut HV M24 10.9		
CONF_09	2	Screw H M12x96-86 10.9 TS FN	Washer 12 300 HV	E1 - S235 J2-1D	CLP 80 KN	E2-S235J2-1D	Washer 12 300 HV		Nut M12 ISO 4032	
CONF_10	1	Screw H M12x96-86 10.9 TS FN	Washer 12 300 HV	E17-S600-1D	Washer 12 300 HV	Nut M12 ISO 4032				
CONF_11	2	Screw H M12x96-86 10.9 TS FN	Washer 12 300 HV	S600-2D	CLP 80 KN	S600-2D	Washer 12 300 HV	Nut M12 ISO 4032		
CONF_12	6	Screw H M12x96-86 10.9 TS FN	Washer 12 300 HV	E17-S600-1D	E4-42CD4 - 2D	CLP 80 KN	E5-42CD4 - 2D	E17-S600-1D	Washer 12 300 HV	Nut M12 ISO 4032

Continued

CONF_14	2	Screw H M12x96-86 10.9 TS FN	Washer 12 300 HV	E1 - S235 J2-1D	CLP 80 KN	E2-S235J2-1D	E11-42CD4-2D-(threaded)			
CONF_15	2	Screw H M12x96-86 10.9 TS FN	Washer 12 300 HV	E18-2024-2D	CLP 80 KN	E18-2024-2D	Washer 12 300 HV	Nut M12 ISO 4032		
CONF_16	6	Screw H M12x96-86 10.9 TS FN	Washer 12 300 HV	E11-2024-2D	CLP 80 KN	E12-2024-2D	E13-2024-2D	Washer 12 300 HV	Nut M12 ISO 4032	
CONF_18	2	Screw H M12x96-86 10.9 TS FN	Washer 12 300 HV	E18-2024-2D	CLP 80 KN	E18-2024-2D	E19-2024-(threaded)			
CONF_19	2	Screw H M12-40 8.8 TS FN	Washer 12 300 HV	E17-S600-1D	CLP 80 KN	E17-S600-1D	Washer 12 300 HV	Nut M12 ISO 4032		
CONF_20	6	Screw H M12-100 8.8 TS FN	Washer 12 300 HV	E17-S600-1D	E4-42CD4 - 2D	CLP 80 KN	E5-42CD4 - 2D	E17-S600-1D	Washer 12 300 HV	Nut M12 ISO 4032
CONF_21	2	Screw Hex-In M12x50 10.9 TS FN	Washer 12 300 HV	E17-S600-1D	CLP 80 KN	E17-S600-1D	Washer 12 300 HV	Nut M12 ISO 4032		
CONF_22	2	Screw Hex-In M12x50 10.9 TS FN		E17-S600-1D	CLP 80 KN	E17-S600-1D	Nut M12 ISO 4032			
CONF_23	2	Screw Hex-In M12x50 10.9 TS FN		E14-GJS600-2D	CLP 80 KN	E14-GJS600-2D	Nut M12 ISO 4032			
CONF_24	2	Screw Hex-In M12x50 10.9 TS FN		E14-GJS600-2D	CLP 80 KN	E14-GJS600-2D	E16-GJS600-(threaded)			
CONF_25	6	Screw Hex-In M12x100 10.9 TS FN		E20-GJS600-1D	E21-GJS600-2D	CLP 80 KN	E21-GJS600-2D	E20-GJS600-1D	Nut M12 ISO 4032	
CONF_27	6	Screw H M12 élégie 10.9 TS FN	Washer 12 300 HV	E23-S600-1D	E24-42CD4-2D C	CLP 80 KN	E25-42CD4-2D P	E23-S600-1D	Washer 12 300 HV	Nut M12 ISO 4032
CONF_28	6	Screw H M12 PF élégie 10.9 TS FN	Washer 12 300 HV	E23-S600-1D	E24-42CD4-2D C	CLP 80 KN	E25-42CD4-2D P	E23-S600-1D	Washer 12 300 HV	Nut M12 ISO 4032
CONF_29	2	Stud DIN 6379 M12-63 10.9	E22-42CD4-(threaded)	Washer 12 300 HV	E17-S600-1D	CLP 80 KN	E17-S600-1D	Nut M12 ISO 4032		

Continued

CONF_30A	2	Stud DIN 6379 M12-63 10.9	Nut M12 ISO 4032	Washer 12 300 HV	E17-S600-1D	CLP 80 KN	E17-S600-1D	Washer 12 300 HV	Nut M12 ISO 4032	
CONF_30B	6	Stud DIN 6379 M12-125 10.9	Nut M12 ISO 4032	Washer 12 300 HV	E23-S600-1D	E24-42CD4-2D C	CLP 80 KN	E25-42CD4-2D P	E23-S600-1D	Washer 12 300 HV
CONF_31	2	Screw H M12x50 A4-80_Vernis	Flat Washer N 12 304	E26-316-1D	CLP 80 KN	E27-316-1D	Flat Washer N 12 304	Nut H M12 A4-80 + STANAL400		
CONF_32	6	Screw H M12x100 A4-80_Vernis	Flat Washer N 12 304	E30-316-2D	CLP 80 KN	E31-316-1D	E30-316-2D	Flat Washer N 12 304	Nut A4 316L 100	
CONF_33	2	Screw H M12x50 A4-80_Vernis	Flat Washer N 12 304	E26-316-1D	CLP 80 KN	E27-316-1D	Flat Washer N 12 304	Self-Locking Nut M12 A4-80		
CONF_34	2	Screw H M12 A8 (1.4529-80)	Flat Washer 12 300 HV BUMAX A4L	E31-316-1D	CLP 80 KN	E31-316-1D	Flat Washer 12 300 HV BUMAX A4L	Nut A4 316L 100		
CONF_35	6	Screw H M12 A8 (1.4529-80)	Flat Washer 12 300 HV BUMAX A4L	E30-316-2D	CLP 80 KN	E31-316-1D	E30-316-2D	Flat Washer 12 300 HV BUMAX A4L	Nut A4 316L 100	
CONF_35B	6	Screw H M12 A8 (1.4529-80)	Flat Washer 12 300 HV BUMAX A4L	E30-316-2D	CLP 80 KN	E31-316-1D	E30-316-2D	Flat Washer 12 300 HV BUMAX A4L	Nut H M12 A4-80 + STANAL400	
CONF_36	6	Screw bi-hex inco718 75.1	Flat WasherA 286	E12-2024-2D	CWF140 kN	E12-2024-2D	Flat WasherA286	Flat WasherA286	Self-Locking Nut Inco 718-Silver Coating	
CONF_37	6	Screw bi-hex inco718 75.1	Flat WasherA 286	E4-42CD4 - 2D	CWF140 kNn	E4-42CD4 - 2D	Flat WasherA286	Flat WasherA286	Self-Locking Nut Inco 718-Silver Coating	

(b)

Ref. Component	Material data					Geometric parameters				
	Young [MPa]	Coef. Poisson	YLS [MPa]	ULS [MPa]	A [%]	fin [mm]	fout [mm]	Th [mm]	S [mm]	Is Threaded
CLP 80 kN (load sensor)	113 072	0.29				14.1	36	5		
CWF140 kN (load sensor)	618 502	0.29				20.9	30.6	13		
E1 - S235 J2-1D	204 000	0.29	386	554	29.5	13	50	6.7	44	
E11-2024-2D	78 000	0.33	365	466	22	13	110	24	100	
E11-42CD4-2D-(threaded)	204 000	0.29	878	1000	18	12	50	30	44	Threaded
E12-2024-2D	78 000	0.33	365	466	22	13	110	19.2	100	
E13-2024-2D	78 000	0.33	365	466	22	13	110	24	100	
E14-GJS600-2D	160 000	0.26	425	720	10.5	13	50	9.6	44	
E16-GJS600-(threaded)	160 000	0.26	425	720	10.5	12	50	24	44	Threaded
E17-S600-1D	245 000	0.29	620	790	21	13	120	9	100	
E18-2024-2D	78 000	0.33	365	466	22	13	50	9	44	
E19-2024-(threaded)	78 000	0.33	365	466	22	12	50	30	44	Threaded
E2-S235J2-1D	204 000	0.29	386	554	29.5	13	50	6.7	44	
E20-GJS600-1D	160 000	0.26	425	720	10.5	13	110	12	100	
E21-GJS600-2D	160 000	0.26	425	720	10.5	13	110	19.2	100	
E22-42CD4-(threaded)	204 000	0.29	878	1000	18	12	50	24	44	Threaded
E23-S600-1D	245 000	0.29	620	790	21	13	120	9	100	
E24-42CD4-2D C	210 000	0.29	643	847	20.5	13	110	19.2	100	
E25-42CD4-2D P	210 000	0.29	643	847	20.5	13	110	24	100	
E26-316-1D	180 000	0.27	249	565	56.6	13	50	6.7	44	
E27-316-1D	180 000	0.27	249	565	56.6	13	50	6.7	44	
E28-M24-S235-2D	210 000	0.29	307	509	32.5	26	110	40	100	
E29-M24-S235-5D	210 000	0.29	307	509	32.5	26	110	66	100	
E30-316-2D	180 000	0.27	249	565	56.5	13	110	19.2	100	
E31-316-1D	180 000	0.27	249	565	56.5	13	120	12	100	
E33-M24-S235-cale	210 000	0.29	307	509	32.5	26	110	12	100	
E3-S235J2-1D	205 000	0.29	307	507	32.5	13	120	12	100	
E4-42CD4 - 2D	210 000	0.29	643	847	20.5	13	110	19.2	100	
E5-42CD4 - 2D	210 000	0.29	643	847	20.5	13	110	19.2	100	
E6-42CD4 - Cale	210 000	0.29	643	847	20.5	13	110	4	100	
E7-S235 J2 -1D	205 000	0.29	307	507	32.5	13	120	12	100	
E8-S355 J2-1D	204 000	0.26	386	554	29.5	13	50	6.7	44	
E9-S355 J2-1D	204 000	0.26	386	554	29.5	13	50	6.7	44	
S600-2D	245 000	0.29	620	790	21	13	50	6.7	44	

To reduce the number of assumptions regarding material properties and friction values, all materials of tested parts have been qualified with basic tensile tests according to ISO 898-part 1 [20] and part 2 (ISO 6892 [21]) for material properties and according to ISO 16047 [19] for friction coefficients values (bearing surface friction coefficient "μ_b" and thread friction coefficient "μ_t").

Table 1 details the experimental program in which we tested different types of fasteners (studs and screws), different product standards (normal, HR and HV bolts), different providers, different materials, different head shapes, different clamped lengths, …

To reduce the operator-effect during tightening, a specific tool has been designed to tighten the tested assemblies using the Torque-Clamp Force Test-bench (#A of Figure 1). This last one applies a regular angle and measures the applied torque. Additional accessories are used to measure screw elongation (LVDT) and bolt force (load sensor). For each configuration, 5 to 10 assemblies have been tested. All tests are performed by the same operator and by using the same equipment, except for M24 assemblies, which require other tools. Finally, all samples are tightened up to the bolt failure.

3.2. Main Experimental Results

Experimental results are treated in two parts: qualification test-results and tightening test results. For the first part, Figure 2 shows the Stress-Strain graph (mean values) of two material specimens from the same batch. Figure 3 shows the linear relationship between the applied torque and the clamp force. It also shows the deviation of the preload due to friction deviation, for a target preload. All experimental results of those tests are summarized in Table 2 and Table 3.

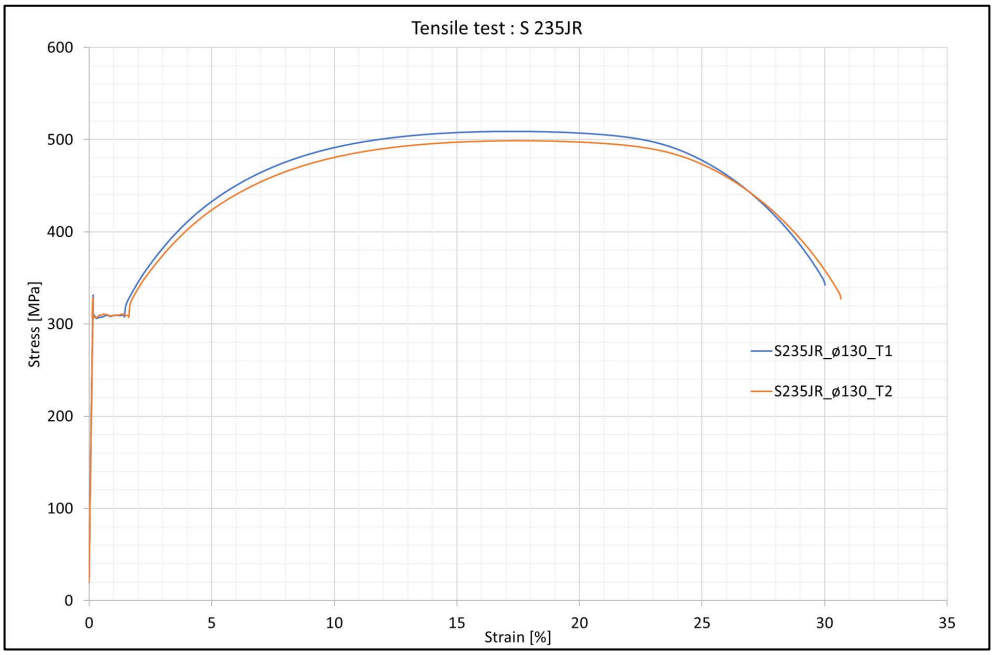

Figure 2. Example of a tensile tests result—material specimen from Clamped parts.

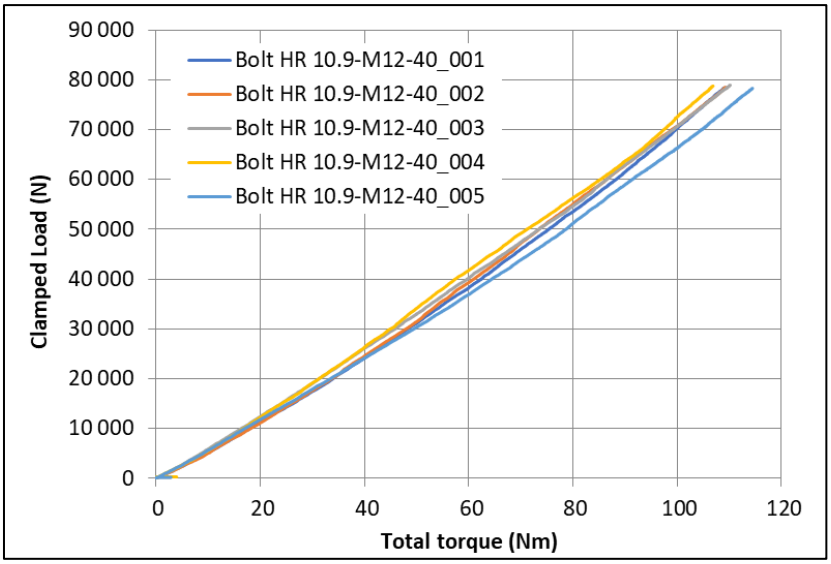

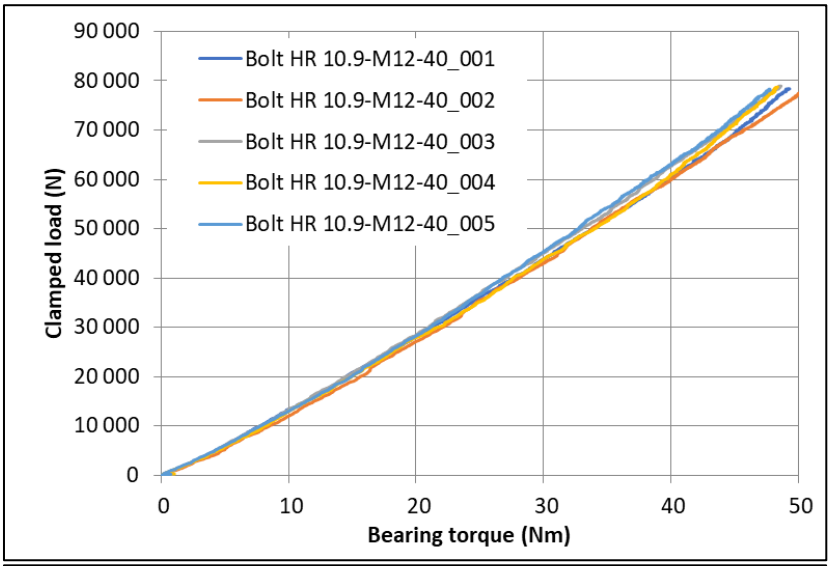

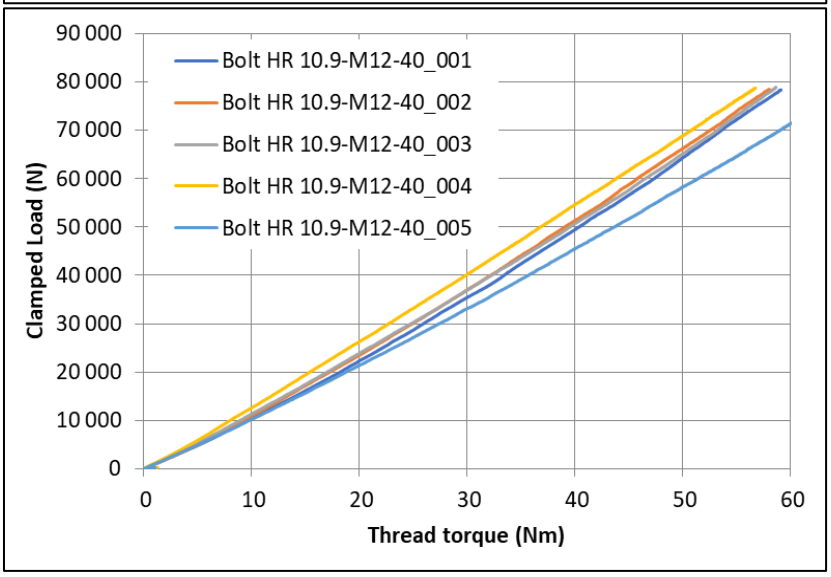

Figure 3. Example of Torque-Clamp Force test for a Friction qualification.

Table 2. Main tensile test results.

Material reference	Test results			
	E (MPa)	YLS (MPa)	ULS (MPa)	A%
Stud DIN 6379 M12-125 10.9	210,000	1009	1098	14
Stud DIN 6379 M12-63 10.9	217,000	828	990	12
Screw bi-hex inco718 75.1	205,000	1700	1800	22
Screw Hex-In M12x100 10.9 TS FN	210,000	1078	1129	14
Screw Hex-In M12x50 10.9 TS FN	210,000	1114	1159	13
Screw H M12 A8 (1.4529-80)	150,000	839	1061	16
Screw H M12 PF élégie 10.9 TS FN	200,000	1030	1062	16
Screw H M12 élégie 10.9 TS FN	210,000	1030	1127	15
Screw H M12-100 8.8 TS FN	210,000	820	913	20
Screw H M12-40 8.8 TS FN	210,000	940	1039	15
Screw H M12x100 A4-80_Vernis	180,000	690	913	20
Screw H M12x50 A4-80_Vernis	180,000	660	885	45
Screw H M12x96-86 10.9 TS FN	210,000	1067	1128	15
Screw HR 10.9 - M12x40	207,000	1085	1129	15
Screw HR 10.9 - M12x80	200,000	1083	1124	18
Screw HV 10.9 - M12-40/25 PGB	207,000	1071	1155	16
Screw HV 10.9 - M12-80/40 PGB	210,000	1117	1189	16
2024 T351	78,000	365	466	22
316L	180,000	249	565	56.5
42CD4 - 130 mm	210,000	643	847	20.5
42CD4-2D (threaded)	204,000	878	1000	18
GJS600	160,000	425	720	10.5
S235 J2-130 mm	205,000	307	507	32.5
S235 J2-60 mm	204,000	386	554	29.5
S600	245,000	620	790	21

Table 3. Main tensile test results.

Configuration reference	Test results		
	Bearing friction (μ_b)	Thread friction (μ_{th})	Comment
Conf 01-(HR-M12-Lk = 2d)	0.07 ± 0.001	0.08 ± 0.006	
Conf 02-(HR-M12-Lk = 6d)	0.08 ± 0.005	0.09 ± 0.008	
Conf 03-(HV-M12-Lk = 2d)	0.10 ± 0.033	0.11 ± 0.018	
Conf 04-(HV-M12-Lk = 6d)	0.08 ± 0.010	0.13 ± 0.024	
Conf 05-(HR-M24-Lk = 2d)	0.07 ± 0.007	0.11 ± 0.009	
Conf 06-(HR-M24-Lk = 6d)	0.07 ± 0.001	0.10 ± 0.005	

Continued

Conf 07-(HV-M24-Lk = 2d)	0.08 ± 0.012	0.12 ± 0.005	
Conf 08-(HV-M24-Lk = 6d)	0.07 ± 0.005	0.13 ± 0.013	
Conf 09-(H-M12-Lk = 2d)	0.11 ± 0.013	0.14 ± 0.007	
Conf 10-(H-M12-Lk = 1d)	0.11 ± 0.013	0.14 ± 0.007	
Conf 11-(H-M12-Lk = 2d)	0.11 ± 0.013	0.14 ± 0.007	
Conf 12-(H-M12-Lk = 6d)	0.11 ± 0.013	0.14 ± 0.007	
Conf 14-(H-M12-Lk = 2d)	0.11 ± 0.013	0.14 ± 0.007	
Conf 15-(H-M12-Lk = 2d)	0.11 ± 0.013	0.08 ± 0.007	
Conf 16-(H-M12-Lk = 6d)	0.11 ± 0.013	0.14 ± 0.007	
Conf 18-(H-M12-Lk = 2d)	0.11 ± 0.013	0.14 ± 0.007	
Conf 19-(Hex In-M12-Lk = 2d)	0.15 ± 0.030	0.15 ± 0.030	Assumption
Conf 20-(H-M12-Lk = 6d)	0.15 ± 0.030	0.15 ± 0.030	Assumption
Conf 21-(Hex In-M12-Lk = 2d)	0.12 ± 0.013	0.14 ± 0.006	
Conf 22-(Hex In-M12-Lk = 2d)	0.12 ± 0.013	0.14 ± 0.006	
Conf 23-(Hex In-M12-Lk = 2d)	0.12 ± 0.013	0.14 ± 0.006	
Conf 24-(Hex In-M12-Lk = 2d)	0.12 ± 0.013	0.14 ± 0.006	
Conf 25-(Hex In-M12-Lk = 6d)	0.12 ± 0.015	0.14 ± 0.007	
Conf 27-(H-M12-Lk = 6d)	0.15 ± 0.010	0.14 ± 0.004	
Conf 28-(H-M12-Lk = 6d)	0.10 ± 0.007	0.13 ± 0.005	
Conf 29-(Stud-M12-Lk = 2d)	0.14 ± 0.004	0.15 ± 0.011	
Conf 30A-(Stud-M12-Lk = 2d)	0.16 ± 0.005	0.15 ± 0.011	
Conf 30B-(Stud-M12-Lk = 6d)	0.15 ± 0.006	0.15 ± 0.010	
Conf 31-(H-M12-Lk = 2d)	0.13 ± 0.045	0.16 ± 0.020	
Conf 32-(H-M12-Lk = 6d)	0.15 ± 0.030	0.15 ± 0.030	Assumption
Conf 33-(H-M12-Lk = 2d)	0.13 ± 0.045	0.16 ± 0.020	
Conf 34-(H-M12-Lk = 2d)	0.08 ± 0.017	0.11 ± 0.025	
Conf 35-(H-M12-Lk = 6d)	0.15 ± 0.030	0.15 ± 0.030	Assumption
Conf 35B-(H-M12-Lk = 6d)	0.15 ± 0.030	0.15 ± 0.030	Assumption
Conf 36-(BH-M12-Inconel-Lk = 6d)	0.15 ± 0.030	0.15 ± 0.030	Assumption
Conf 37-(BH-M12-Inconel-Lk = 6d)	0.15 ± 0.030	0.15 ± 0.030	Assumption

The second part of results (tightening tests) is presented and discussed in this section and in the validation section of this paper.

Using configuration 1 (clamped length "L_k" ~ $2d$ where "d" is the nominal diameter), Figure 4 shows the evolution of preload regarding bolt elongation. It shows a large plastique area for HR bolts. This area is mainly defined by the physical and geometrical properties of the tested bolt. We note also some deviations in the elastic area, which could be due to the quality of the contact between the bolt and used sensor LVDT.

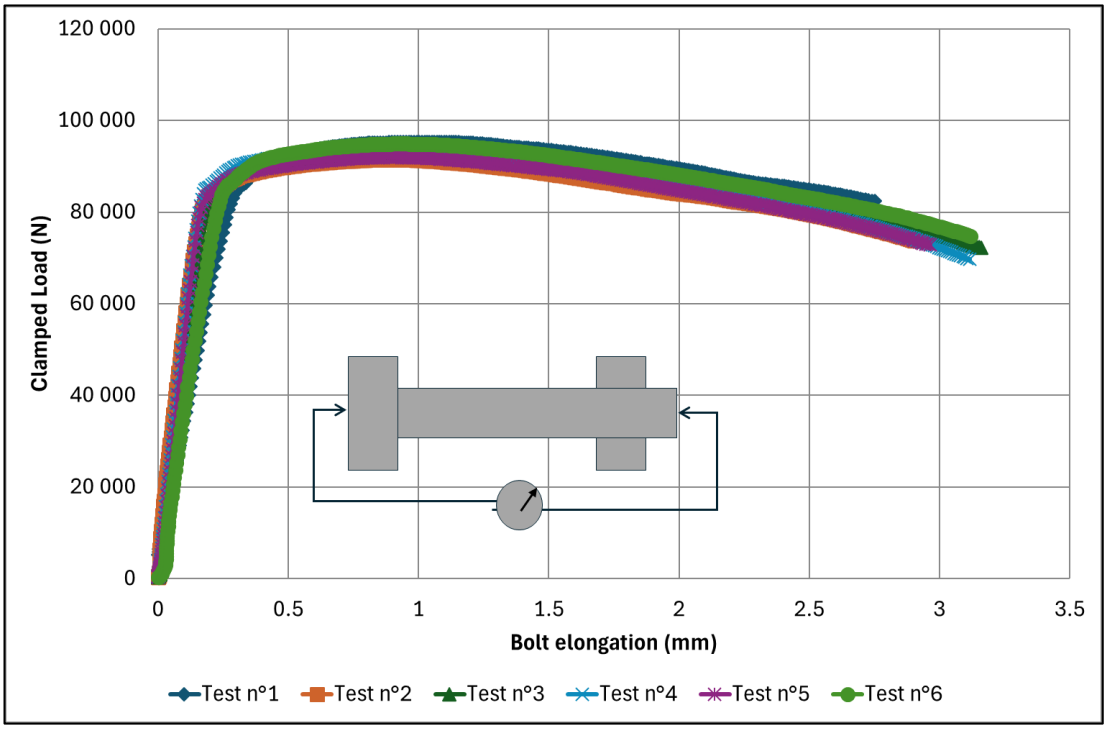

Figure 4. Example of a Preload-Bolt elongation: Case of HR M12 bolts.

Graph in **Figure 5** gives an example of a bolt elongation (mean values) during the tightening operation. It shows a linear relationship between bolt elongation and applied angle, as well as non-linear behaviors at the start and end of the tightening tests. The first non-linearity is due to the contact between the sensor LVDT and the bolt, and the initial gap at the engaged threads. The second is due to the beginning of the thread stripping (for this case) or bolt yielding.

For the tested configuration shown in **Figure 5**, by ignoring snugging angle (non-linear behavior), the theoretical rotation of the nut is estimated to $\Delta\theta = \frac{\Delta L_b}{P} \times 360 = \frac{3.3-0.6}{1.75} \times 360 = 555.4^\circ$ (according to Equation (5)). This rotation is significantly lower than the measured angle ($662.3^\circ - 40.6^\circ = 621.7^\circ$). This difference is mainly due to the tool resilience (stiffness) and its accessories (sockets, extension…). It demonstrates that the real assembly is more flexible than the calculated one (theorical assembly). And it confirms the existence of an additional resilience (**Table 2**). This conclusion is mentioned by Fukuoka [10] and Gold [11]. The first author improved the resilience formula by adding a non-linear contact resilience. The second gives other explanations based on the local stress and the elasto-plastic properties of the material, which will be investigated later. In fact, and according to two different papers of Fukuoka ([10] and [20]), we can see a good correlation between theorical approach and experimental results. But in the first paper, he considers the roughness effect on the additional contact resilience, and he ignores this factor in his second work (based on a specific axisymmetric FEA model).

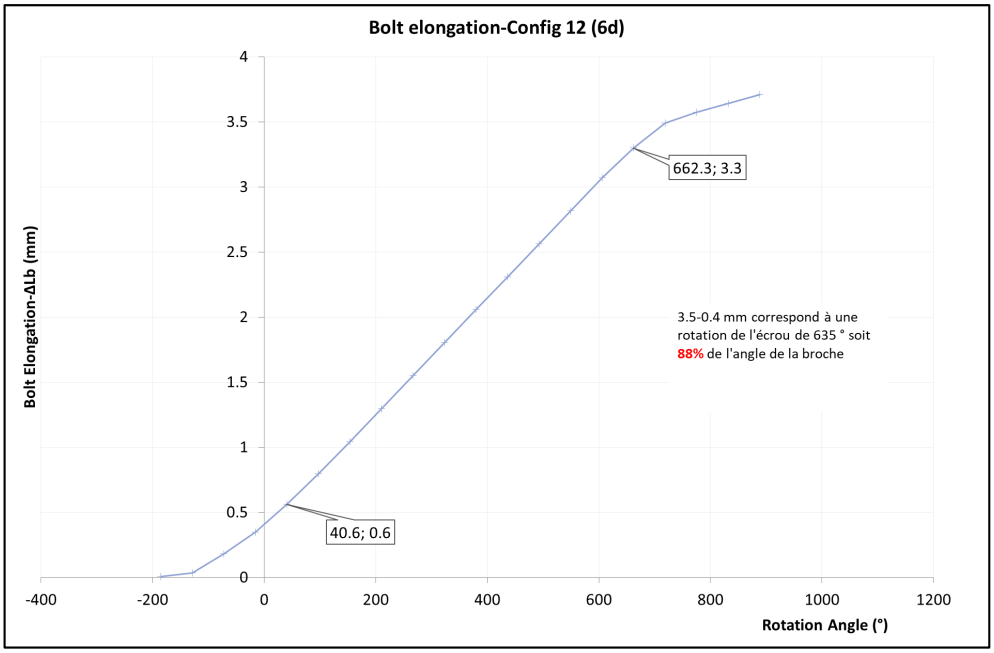

Figure 5. Bolt elongation during the tightening of conf. #12 (bolted joint M12, $L_k = 6d$).

Graphs of **Figure 6** and **Figure 7** illustrate the importance of the resilience (stiffness) of the bolt and clamped parts, defined mainly by the length and the Young modulus. It shows that the higher the clamped length ratio (L_k/d), the more the bolt has to be turned to install required preload. This reduces the sensitivity of the angle factor on the applied preload. In fact, for a stiff assembly (L_K close to $2d$), any error of ±10 degrees on applied angle introduces a preload deviation of ±10 kN against ~±5 kN in the case of a highly elastic assembly ($L_k = 6d$).

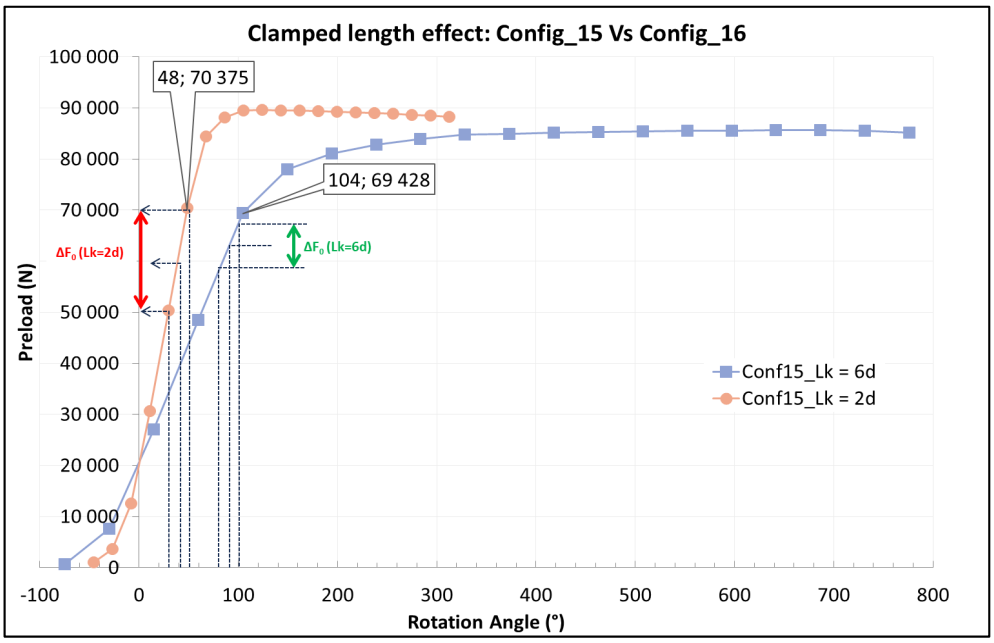

Figure 6. Evolution of applied load during nut rotation—case of 2 different clamped lengths.

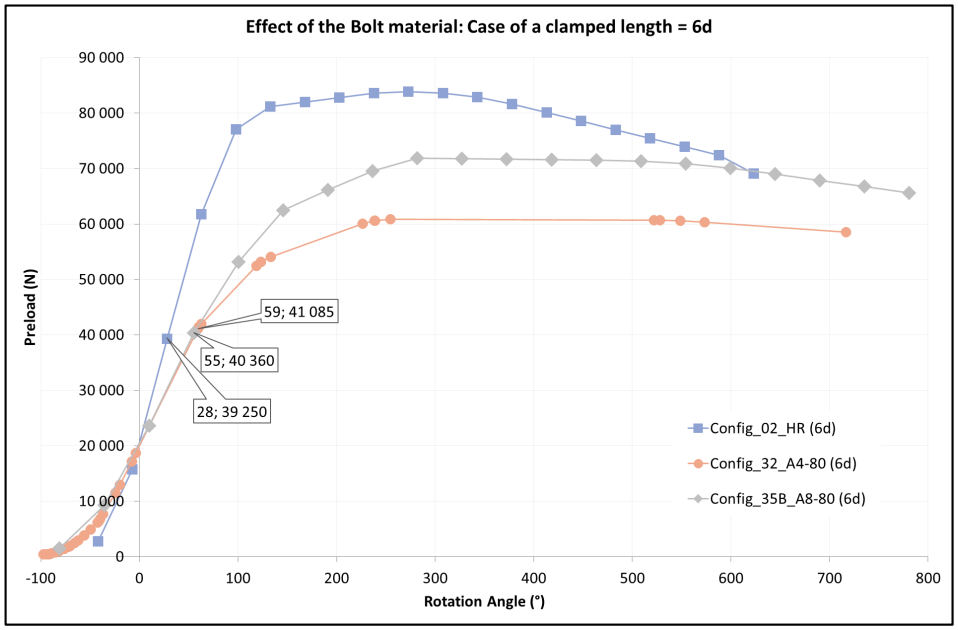

Figure 7. Evolution of applied load during nut rotation - case of different part-materials.

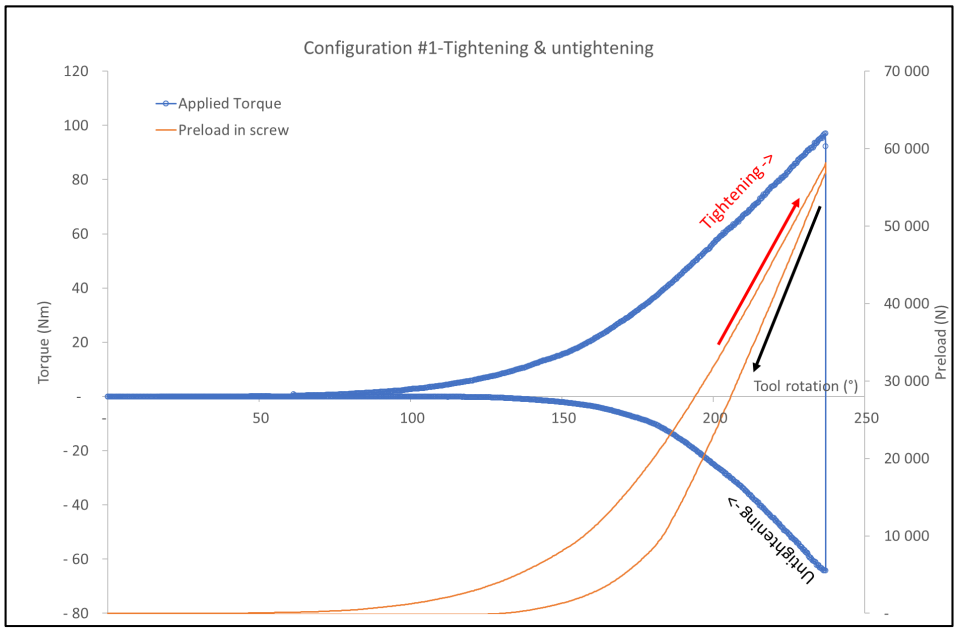

Figure 8. Tightening and untightening steps of a bolted joint M12 (Config. #1).

The graphs in **Figure 8** show the evolution of applied torque and introduced load as a function of applied angle. From those graphs we can note:

- The tightening step is defined by two types of behaviors: a non-linear behavior "Torque-Angle" and "Preload-Angle", and linear behavior before any yielding phenomenon. These graphs demonstrate the importance of the snug torque in the beginning of the tightening where the relationship between the applied torque and introduced angle is non-linear.
- The untightening step has a different slope "Preload-Angle" compared to the

tightening step. This demonstrates that the typical formula used to qualify the relationship between angle and preload ($\Delta F_0 = \frac{P \times \Delta\theta}{360 \times (\delta_b + \delta_p)}$) is wrong. This is due to there being no evolution of resiliencies or thread Pitch between the tightening and untightening steps.

The graphs of Figure 9 show a limited effect of the thread pitch on the applied angle. In fact, the use of a fine pitch increases the required angle to introduce a similar load compared to a coarse pitch. This effect may be more significant in the case of a stiff assembly. Indeed, for a clamped length $L_k = 6d$, to introduce 39.6 kN, using a fine pitch (1.5 mm) increases the required angle by only 4˚ (36˚ instead of 32˚).

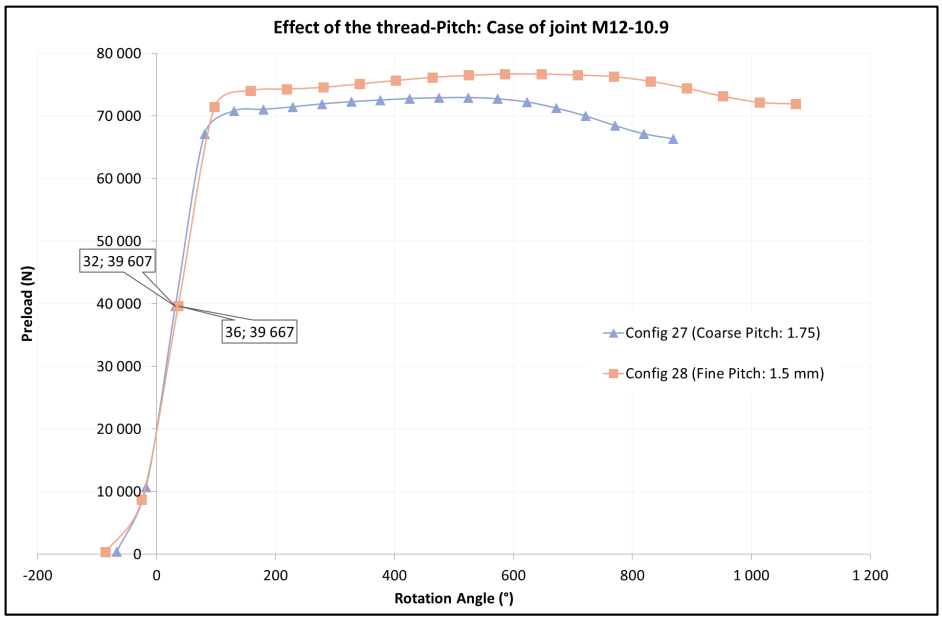

Figure 9. Effect of the pitch on a combined tightening (bolted joint M12, $L_k = 6d$).

The graphs in Figure 10 show the same behavior of two similar assemblies where only the nut has been modified. It demonstrates that for a snug torque higher than the locking torque, the combined tightening can ignore the locking torque effect. But for higher locking torque, this observation may be wrong.

Finally, using test-results of the Torque-Clamp Force qualification according to ISO 16047 (Bolt HR 10.9 M12x40), we can note a significant evolution of the basic relationship between bolt preload and Torques (bearing surface torque, thread torque and total torque) after the yielding of the bolt as shown in Figure 11. According to these graphs, the linear relationship between torques and bolt preload is only valid before the yield point of the bolt. This means the friction coefficient at the bearing surface (Figure 11(c)) and on the threads (Figure 11(d)) decreases after bolt yielding. In this paper, this evolution will be ignored by the proposed model (below) when extended to plastic tightening. And it will be developed in future work.

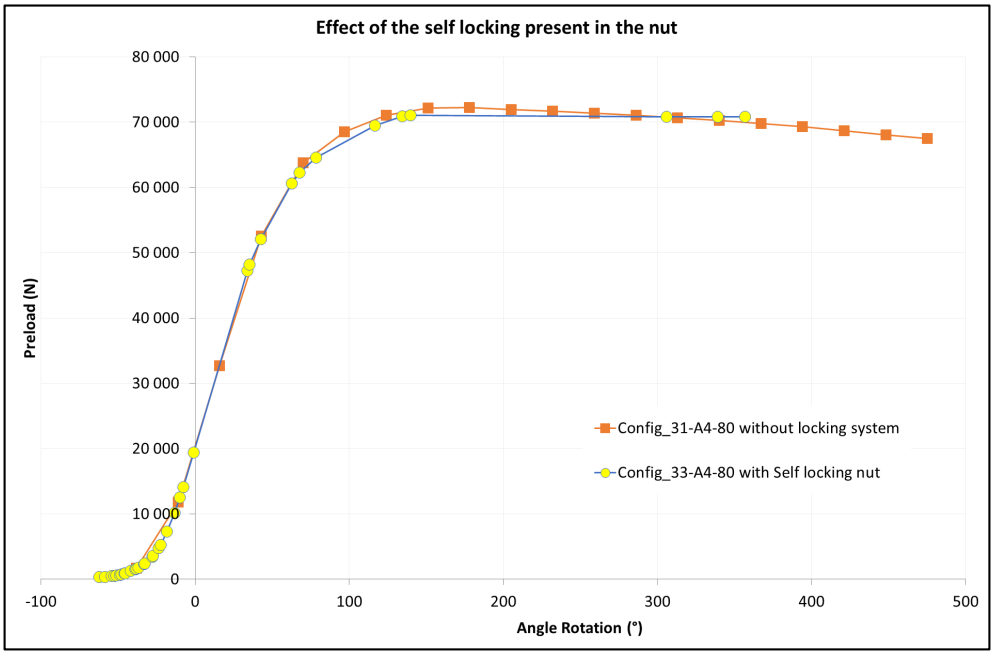

Figure 10. Effect of the locking torque on combined tightening (bolted joint M12, $L_k = 2d$).

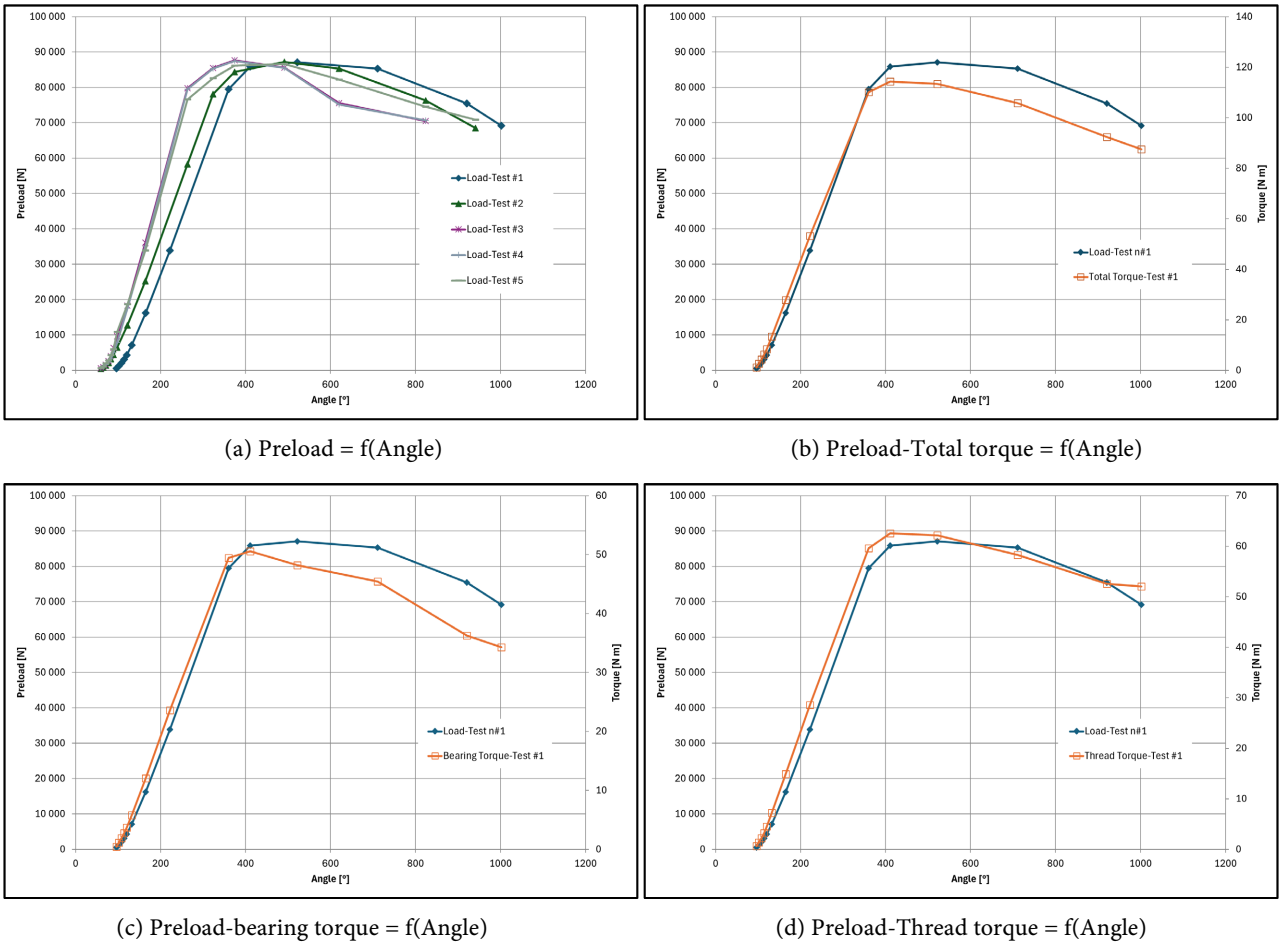

(a) Preload = f(Angle)

(b) Preload-Total torque = f(Angle)

(c) Preload-bearing torque = f(Angle)

(d) Preload-Thread torque = f(Angle)

Figure 11. Comparatives evolutions of bolt preload and torques as a function of turned angle.

4. Improvement of Existing Formulas

In this section, we detail some of the improvements made to existing formulas, taking into account the previous analysis.

4.1. Improvement of the Preload-Angle Formula

Figure 12 illustrates the difference between the measured angle and the effective angle, which generates a relative rotation between the nut and the bolt. We can note that the measured angle is the sum of 3 different rotations.

$$\Delta\theta = \Delta\theta_{tool} + \Delta\theta_{b,Torsion} + \Delta\theta_{u} \tag{9}$$

1) $\Delta\theta_{tool}$: Torsion rotation (angle) of the tool and its accessories. Some automatic screw drivers compensate for this quantity. At the end of this paper, we propose a simplified way to qualify the tool stiffness/resilience.

$$\Delta\theta_{tool} = \frac{\Delta T}{K_{tool}} = \Delta F_0 \times \left(\frac{P}{2\pi} + 0.577 \times d_2 \times \mu_t + \frac{D_b}{2} \times \mu_b \right) \times \delta_{tool} \tag{10}$$

2) $\Delta\theta_{b,Torsion}$: Torsion rotation (angle) of the bolt. The torsion resilience/stiffness of the bolt can be calculated in the same way as axial and bending resilience.

$$\Delta\theta_{b,Torsion} = \frac{T_{thread}}{K_{b,Torsion}} = \Delta F_0 \times \left(\frac{P}{2\pi} + 0.577 \times d_2 \times \mu_t \right) \times \delta_{b,t} \tag{11}$$

3) $\Delta\theta_{u}$, useful angle

$$\Delta\theta_{u} = \frac{\Delta F_0}{K_{\theta}} = \Delta F_0 \times \frac{360 \times \left(\delta_b + \delta_p \right)}{P} \tag{12}$$

With Equations (8) to (12), we can deduce the final formula (13).

$$F_0 = \frac{T_{sung}}{\frac{P}{2\pi} + 0.577 \cdot d_2 \cdot \mu_t + r_b \cdot \mu_b} + \frac{\Delta\theta}{\frac{360 \cdot \left(\delta_b + \delta_p \right)}{P} + \left(\frac{P}{2\pi} + 0.577 \cdot d_2 \cdot \mu_t \right) \cdot \delta_{b,t} + \left(\frac{P}{2\pi} + 0.577 \cdot d_2 \cdot \mu_t + \frac{D_b}{2} \cdot \mu_b \right) \cdot \delta_{tool}} \tag{13}$$

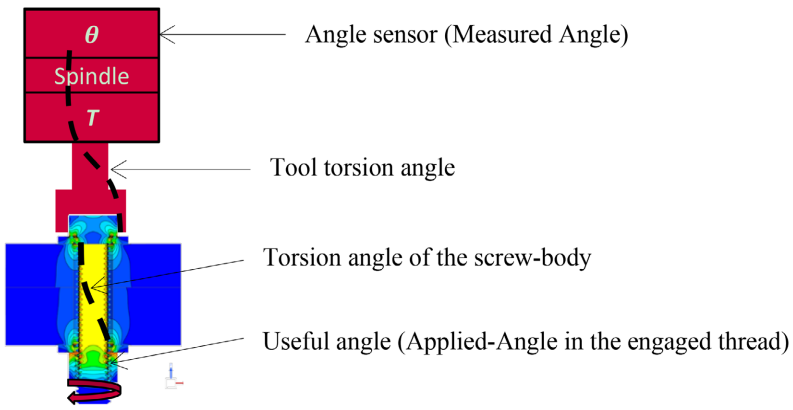

Figure 12. Applied and measured tightening-Angle.

This final formula shows all the factors influencing the relation between the bolt preload, snug torque and the applied angle ($\Delta\theta$). It adds the effect of friction, and additional factors that may be ignored in some cases.

4.2. Improvement of Clamped Part-Resilience Formula

Based on the results of Gold [11] and of Fukuoka [22], we have performed an axisymmetric FEA model (**Figure 13**). We were interested in the evolution of part compression under a tightening load of 59.6 kN. The graph of **Figure 14** shows the evolution of the axial displacement of the parts at the hole from the head (axial position $Z = 22$) to the nut (axial position $Z = 62$). It shows that a significant portion (more than 50%) of part compression is obtained with two local areas located at the interface in contact with the fastener up to a depth of 6 mm.

According to VDI 2230 approach, the part compression is detailed in **Table 4**.

Table 4. Calculation of the axial resilience of clamped parts.

Input data	D_P (mm)	L_k (mm)	D_w (mm)	D_h (mm)	E_P (MPa)
	60	40	16.63	13.5	210,000
Calculated data	$D_P^* = \frac{D_P}{D_w}$	$L_k^* = \frac{L_k}{D_w}$	$\tan\varphi = 0.362 + 0.032\ln\left(\frac{L_k^*}{2}\right) + 0.153\ln D_p^*$		Cone angle (°)
	3.61	2.41	0.5642		29.43°
Total part resilience (mm/N)			$\delta_P = 2\times\frac{\ln\left[\frac{(d_w + D_h)\times(D_w + L_k\times\tan\varphi - D_h)}{(D_w - D_h)\times(D_w + L_k\times\tan\varphi + D_h)}\right]}{E_p\times\pi\times D_h\times\tan\varphi}$ $= 6.154\text{e}-7$		

Using the preload and the FEA displacement at the hole edge, the local resilience is calculated at 1.29e−6 mm/N. Using the preload and the difference between the mean displacement under the bearing surfaces (bolt head and under the nut), the mean FEA resilience is equal to 9.36e−7 mm/N, that is closer to the analytical calculated resilience.

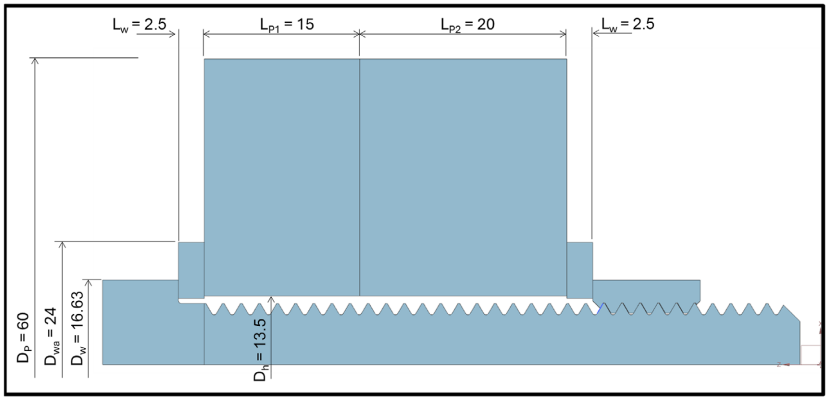

Figure 13. FEA analysis-description of analyzed assembly.

Due to the difference between analytical and FEA results, we can assume that the part resilience to be used during tightening is different to that used for load factor calculations. According to Alkatan [7] and Massol [8], the part resilience calculation is based on elastic energy of the part. This resilience gives only a mean part-compression. With regard to the surface contact between bolt head and part, we can assume that this contact is a Herz contact. As a consequence, the full parts resilience during tightening can be calculated by Equation (14).

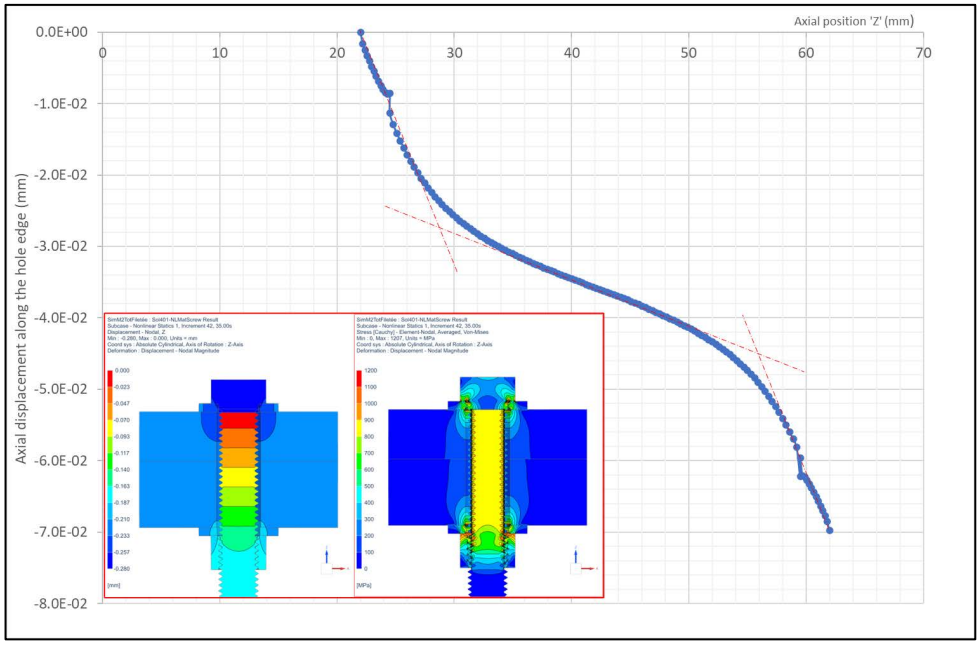

Figure 14. FEA analysis-evolution of part compression at the bolt hole.

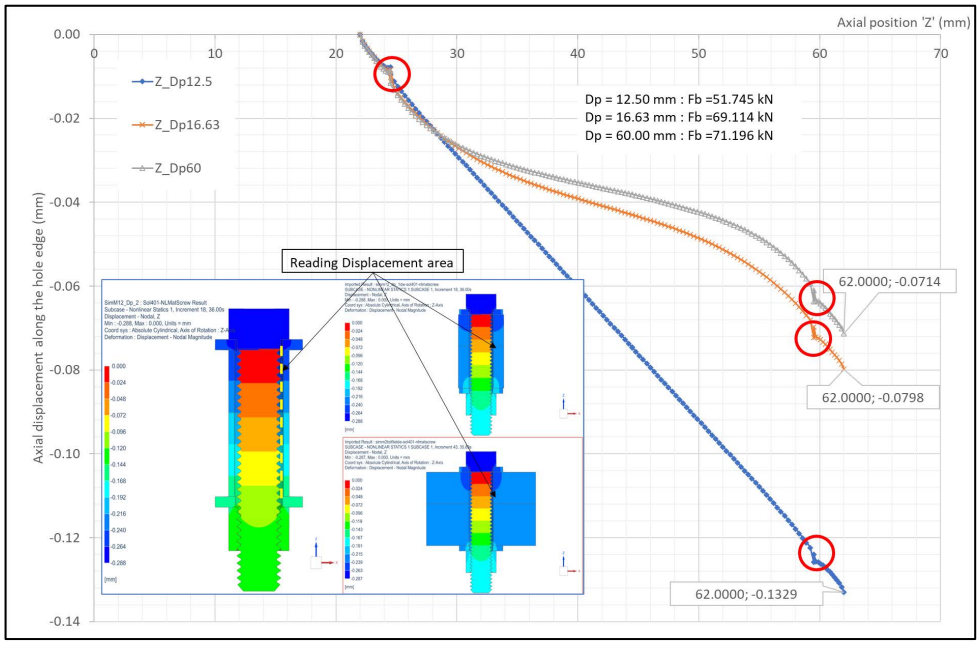

Figure 15. FEA analysis-evolution of part compression along the bolt hole: cases of 3 D_p.

Figure 14 and Figure 15 demonstrate that the compression of the clamped parts is defined by a mixture of Hertzian and normal elongations.

$$\delta_P = \sum \delta_{P,Elastique(NFE,VDI,\cdots)} + \sum \delta_{P,Hertz} \tag{14}$$

$$\delta_{P,Hertz} = \frac{1-\nu^2}{D_{w,eq} \times E_{eq}} \tag{15}$$

Where equivalent Young modulus

$$E_{eq} = \frac{1}{\frac{1}{E_{P,i}} + \frac{1}{E_{P,i+1}}} \tag{16}$$

And Equivalent diameter:

$$D_{w,eq} = \sqrt{d_w^2 - d_h^2} \tag{17}$$

Finally, the simplified method consists of calculating the parts resilience according to the basic approach (VDI 2230 [1], Alkatan [7], Massol [8], Bickford [23] or Rasmussen [24]...) and adding Hertz resilience for the smallest contact surfaces.

4.3. Calculation of Maximal Snug Torque to Achieve Target Accuracy

Today, maximum snug torque is defined by experience or by practical rules. These rules specify 25% to 30% of maximal target preload should be introduced by the snug torque.

In this section, we determine the maximal snug torque to achieve any final tightening factor ("α" as defined by VDI 2230 [1] and Equation (18)). At first, we suppose the maximal preload "F_0^+" and tightening factor "α" are known (e.g. $F_0^+ = 80\%$ YLS and $\alpha = 1.4$), then we calculate the required snug torque.

The deviation of the final preload (introduced by angle and by the snug torque) and of snug preload can be calculated respectively by Equation (19) and Equation (21). The combination of Equation (18) and Equation (21) defines the maximum preload to be introduced by the snug torque (Equation (22)). Finally, the snug torque (Equation (23)) can be calculated using any formula describing the relationship between torque and preload (ISO 16047 or equivalent).

$$\alpha = \frac{F_0^+}{F_0^-} \tag{18}$$

$$\Delta F_0 = F_0^+ - F_0^- = \left(1 - \frac{1}{\alpha}\right) \times F_0^+ \tag{19}$$

$$\alpha_{sung} = \frac{F_{0,snug}^+}{F_{0,snug}^-} \tag{20}$$

$$\Delta F_{0,snug} = F_{0,sung}^+ - F_{0,sung}^- \le \Delta F_0 \tag{21}$$

$$F_{0,snug}^{+} \le \frac{\left(1-\frac{1}{\alpha}\right)}{\left(1-\frac{1}{\alpha_{sung}}\right)} \times F_{0}^{+} \tag{22}$$

$$T_{sung} = \frac{F_{0,sung}^{+}}{1+\frac{\Delta T}{T}} \times \left(\frac{P}{2\pi} + 0.577 \times d_2 \times \mu_{th} + \frac{D_b}{2} \times \mu_b\right) \tag{23}$$

Equation (22) demonstrates the importance of the snug torque accuracy, on the final preload accuracy. For industrial applications, the snug-tightening factor can be estimated at 2 ($1.5 < \alpha_{sung} < 2.5$) and the final tightening factor for combined tightening is estimated between 1.2 and 1.4. In this case, the snug torque/preload should not exceed 33% to 57% of the final Torque or Preload.

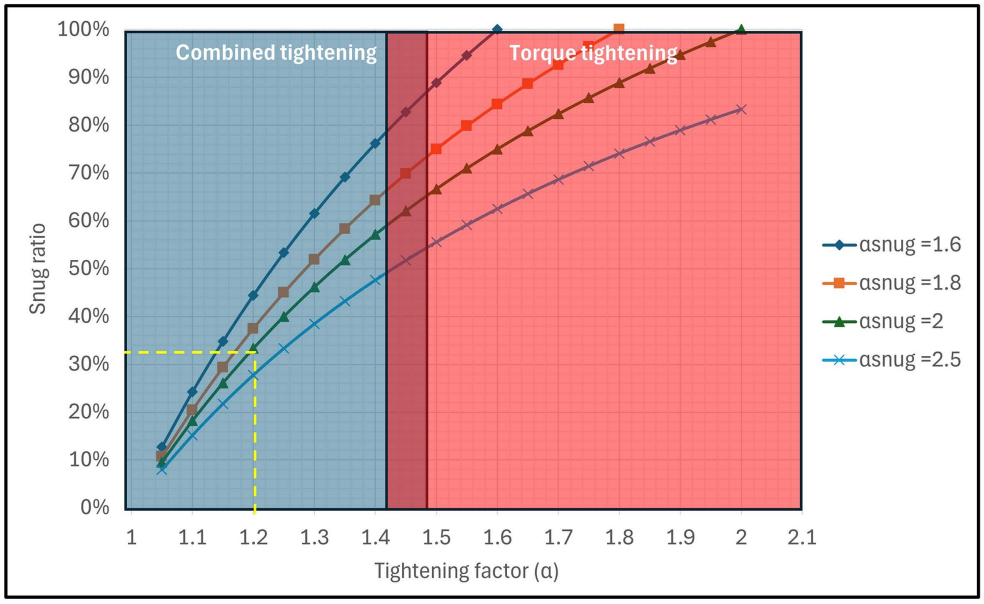

Figure 16. Evolution of the snug ratio ($F_{0,snug}/F_0$) as a function of the snug and target tightening factors (α_{Snug} and α).

According to the graph in **Figure 16** (Equation (22)), an accurate tightening using combined tightening ($\alpha < 1.1$), requires a very low snug ratio. However, using a low snug ratio could cause the tightening preload to fall within the non-linear range of the angle-preload relationship, which is another source of final preload-deviation. In other case, for a higher level of the tightening factor, the snug-Preload could be closed to the target preload (e.g. $\alpha_{sung} = \alpha = 1.6$). In this case, combined tightening offers no advantage.

4.4. Experimental Qualification of the Stiffness of the Tightening Tool

To measure the stiffness of the tightening tool and its accessories (socket, extension, adapters…), several experimental ways can be used. Below, we propose a

simplified method which can be used. It consists of recording the torque and the angle during the bolt tightening at any torque-level (close to the bolt's maximum capacity) and during the untightening step, as shown in Figure 17.

The torsion stiffness of the tool used to tighten the bolt is determined by the "torque-angle" slope during the untightening (or re-tightening) operation before any relative rotation between the nut and the screw. In our case, the stiffness of the tightening tool, as shown in Figure 17 (during the untightening step), is equal to 24 Nm/°.

This stiffness should be ignored when using a servo-controlled screwdriver, which anticipates this additional rotation due to its accessories.

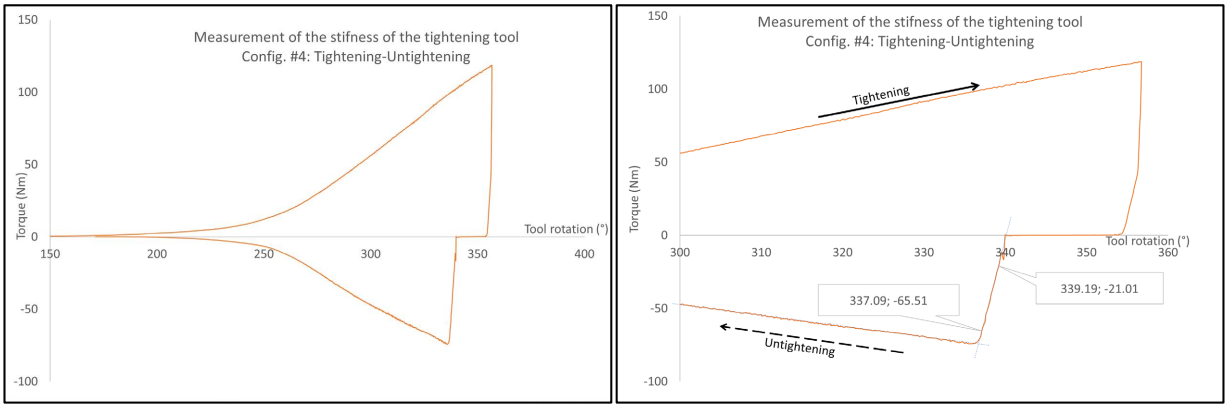

Figure 17. Measurement of the tightening tool stiffness and its accessories.

4.5. Extension of Work for a Tightening after the Yield Point

The tightening after the yield point consists of tightening bolts beyond their elastic capacities. This leads to strain hardening of the screw material (on its critical/threaded area). Friedrich [12] presented a simplified approach to define the angle and the snug torque for this kind of tightening. The tightening after the yield point allows for a significant deviation in the applied angle and reduces the effect of any inaccuracy in the snug torque.

In our study, we adjusted the existing approach using the real S-S curve of the bolt.

This extension is described by the calculation steps detailed below:

1) We transform the body of the fastener into a set of cylinders or shanks (threaded and unthreaded shanks).

2) For any target preload "F_0", we calculate the relative nut-bolt rotation as described below:

a) We calculate the equivalent (Von Mises) stress (combination of axial and torsional stress) in any critical shank.

b) Using Neuber correction and bolt stress-strain curve, we calculate the real stress and strain in the critical shank.

c) From the calculated "real stress", we calculate the residual preload.

d) From the calculated strain, we calculate the shank elongation.

e) We perform the same calculation for all other shanks using the residual preload.

f) The total bolt elongation can be calculated by summing all shank-elongations.

g) Using the parts resilience and the residual preload, we calculate the clamped-parts elongation.

h) Finaly, the nut rotation " θ_{F_0} " can be calculated using the bolt and parts elongations, torsion angle of the bolt-body and the additional angle introduced by tightening-tool-accessories.

2) With the snug torque " T_{snug} ", we calculate the snug preload by using the ISO 16047 formula (formula 2 [19]).

3) We perform the same calculation for the snug preload " T_{snug} " (step 2) to calculate the snug angle " θ_{snug} ".

4) Finally, the final combined tightening will be defined by " $T_{snug} + \Delta\theta$ ", where the final angle to be applied is defined by Equation (24).

$$\Delta\theta = \theta_{F_0} - \theta_{sung} \tag{24}$$

This extension will be developed in another paper discussing the fatigue behavior of yielded assemblies, where S. Gold [11] demonstrated the performance of these assemblies in this case.

5. Experimental Validations of the New Formulas

To validate this work, we have developed a numerical tool and a database containing all experimental data, sample parameters (geometric and material data) and all configuration definitions. This tool calculates all required factors and plots theoretical "preload-angle" curves according to our detailed development. Then it adds the experimental curves to the same graph. It optimizes the number of points to plot the experimental results by reducing the linear area to two points that define the beginning and the end of this area with an accuracy of less than 2%.

Due to the high number of tightening tests performed for each configuration, and to improve the graphs quality, only statistical curves (average and average ±2 Std.Deviation) will be presented to summarize the experimental results for each tested configuration. For the theoretical curves, only maximal and minimal preload-angle curves will be plotted to evaluate the performance of this model. The maximum and minimum levels of preload (F_{0_Max} and F_{0_Min}) are calculated respectively by these combinations (maximum level of snug torque and minimum level of frictions) and (minimum level of snug torque and maximum level of frictions).

To amplify the error between the experimental results and the calculated results, we consider a zero deviation of the preload from the snug torque for the experimental results (for all tests), the zero angle will be set when preload is equal to 20 kN for M12 et 50 kN for M24.

Finally, to plot the graphs below, we used:

- A snug preload for all tested configurations: ~25% YLS x A_s.

- Torque tightening accuracy (to apply the snug torque): ±10%.
- Additional tightening tool stiffness: 24 Nm/˚ (see §4.4).
- Default friction coefficient used for the configuration where the Torque-Clamp Force relationship was not qualified: 0.15 ± 0.03.
- Minimal YLS and ULS values according to ISO 898-1 [20] for bolt and studs which no Tensile test was performed.
- A theoretical bi-linear material for most bolts that hadn't been qualified according to IS0 898-1.

The theoretical curves are obtained by gradually increasing the target preload. **Appendix 1** presents all the comparative graphs between the calculated preload (F_{0_Max} and F_{0_Min}) and the experimentally measured preload (Exp. Avg, Exp. Avg. + 2stdDiv and Exp. Avg. - 2stdDiv, where Avg. means the average value of all tested specimens and stdDiv is the standard deviation) as shown in **Figure 18**.

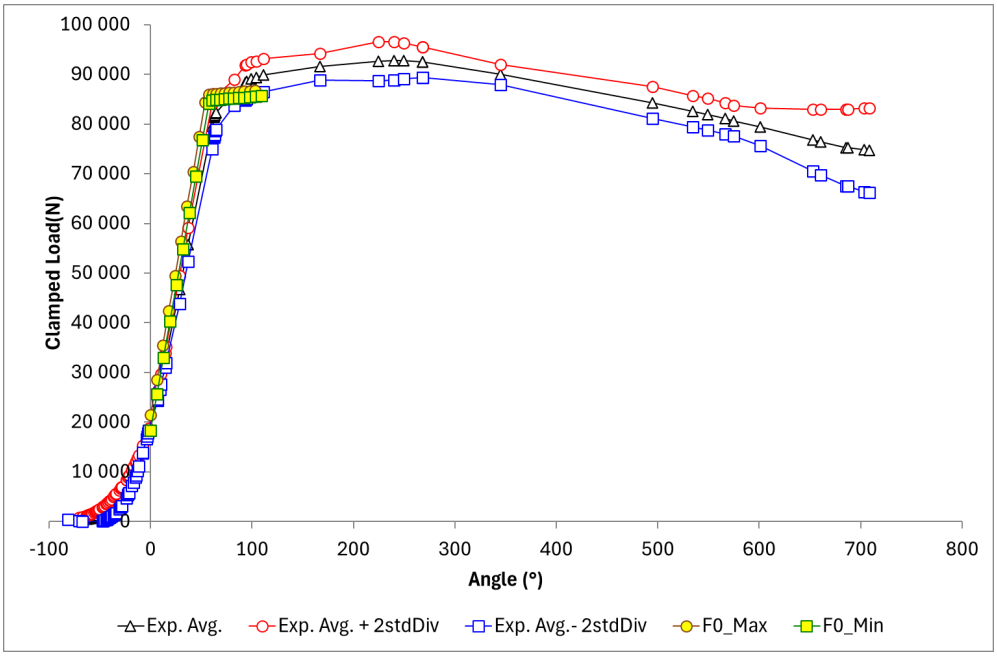

Figure 18. Example of validation graph (Conf 01: HR-M12-Lk = 2d).

For almost all tested configurations, the theoretical and experimental graphs overlap. This illustrates the reliability of the proposed approach.

The theoretical and experimental results confirm basic recommendations used for combined tightening, as reminded below:

1) Use of an "elastic" assembly by increasing the ratio L_k/d (clamped length / nominal diameter). This rule is confirmed by many tested configurations (e.g. Conf 01 & 02; 03 & 04; 10, 11 & 12,…) which illustrate that the required angle for any specified Preload is greater for a higher ratio. This means that any deviation from the applied angle results in a limited deviation from the preload.

2) Using a snug torque to introduce ~20% to 30% of the final preload. This rule is demonstrated by all tests, which show a non-linear relationship between the

applied angles and the preload.

3) Accurate combined tightening is achieved by tightening after the yield point. This rule is illustrated by the horizontal slope for assemblies with a ratio $L_k/d = 6$. In reality, after the yield point and before damaging the bolt (ULS), all applied angle is transformed into metal strain hardening without any significant evolution of the preload.

Finally, the graphs presented in the appendix demonstrate the performances of the proposed model for any elastic combined tightening. To use this model for yielding tightening after the yield point, the user must:

a) Use accurate stress-strain curves for their bolts.

b) Use accurate (measured) friction values on the bearing surface and on the threads.

c) Use stiff tools and accessories. Else, it is necessary to measure the tool stiffness.

Figure 19 gives a comparative graph between existing ("Old") and improved formula ("New"). It shows the effect of the Hertzian resilience and the additional resilience coming from tool accessories. By limiting analysis to linear area and using the worst configuration for a combined tightening ($L_k = 2d$), Figure 19 shows that the "Old" approach overestimates clamped load at 36%, that was mentioned approximately by GOLD [11]. In addition, it shows that, the improvement of the calculation of part resilience reduces significantly the gap between analytical and experimental results (10%). In other words, by adding Hertzian effect, the part resilience is highly increased (3.73×10^{-7} - 1.45×10^{-6} mm/N).

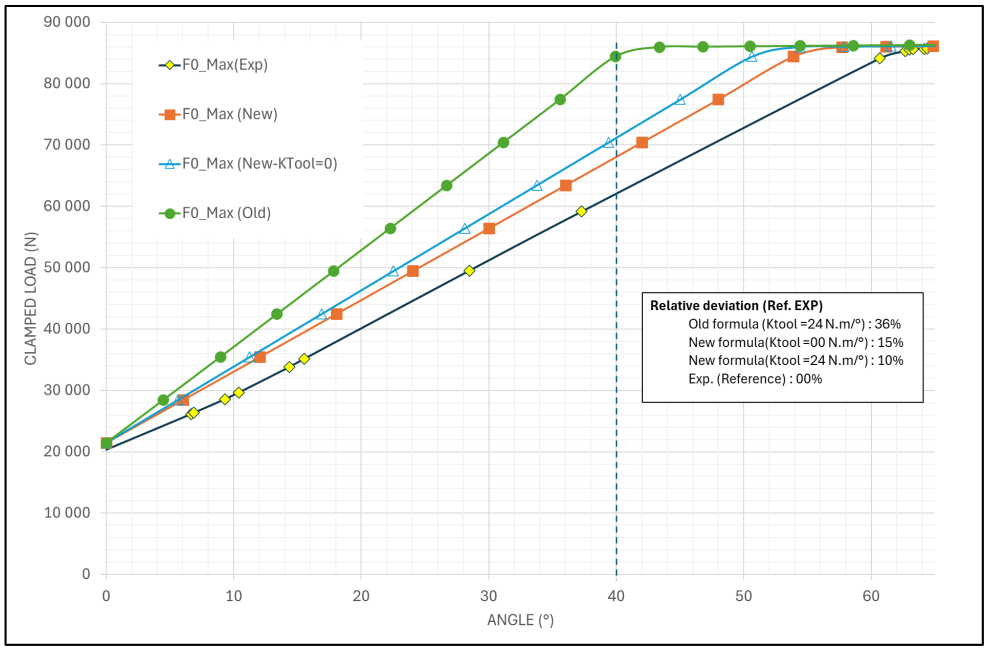

Figure 19. Comparative analysis between old and proposed formulas (Conf 01: HR-M12-$L_k = 2d$).

6. Conclusions

This paper discusses combined Torque-Angle tightening. It provides a new ana-

lytical approach that takes into account local and Hertzian contacts under the fastener bearing surfaces (bolt head or nut) or other small surfaces, additional rotation (torsion angle) due to the tool and its accessories, which could be ignored when using very stiff tools, as well as the elastoplastic behavior of the bolt. These improvement factors are demonstrated by numerical and experimental analysis.

An extensive experimental study was performed with more than 37 tests, each involving 5 to 10 tightening operations (without any reuse of bolts). In addition to the tightening tests, other qualification tests were performed: material properties (tensile tests according to ISO 898-1 and ISO 6892-1) and qualification of friction coefficients (thread friction coefficient and bearing surface friction coefficient with Torque-Clamp force test according to ISO 16047).

Despite the simplified qualification of tool stiffness, the validation curves demonstrate the performance of the new proposed formula to improve the preload accuracy on bolted assemblies when using combined Torque-Angle tightening.

Finally, this paper proposes another way to calculate maximum snug torque in order to achieve the target preload accuracy (or target tightening factor).

Conflicts of Interest

The authors declare no conflicts of interest regarding the publication of this paper.

References

[1] VDI 2230 (2014) Systematische Berechung Hochbeanspruchter Schrauben-verbindungen Zylindrische Einschraubenverbin-dungen.

[2] NF E 25030 (2014) Fixations—Assemblages vissés à filetage métrique ISO—Partie 2: Règles de conception pour les assemblages précontraints—Démarche complète.

[3] NF EN 1993-1-8 (2024) Eurocode 3—Design of Steel Structures—Part 1-8: Joints.

[4] NF EN 1090-2 (2020) Execution of Steel Structures—Technical Requirements for Steel Structure—Part 2/CN: National Addition to NF EN 1090-2.

[5] Durand, A. (1995) Rapport d'étude Cetim 175630—Comparaison de deux méthodes de serrage.

[6] Guillot, J. (1997) Assemblages par éléments filetés. Modélisation et calcul: Techniques de l'Ingénieur BM 5 563.

[7] Alkatan, F. (2005) Modélisation des raideurs des assemblages par éléments filetés précontraints. Master's Thesis, INSA de Toulouse.

[8] Massol, J. (1998) Étude des assemblages boulonnés à chargement faiblement ex-centré soumis à des sollicitations de fatigue. Master's Thesis, INSA de Toulouse.

[9] Bikford, J.H. (1998) An Introduction to the Design and Behaviour of Bolted Joints. Marcel Dekker Inc.

[10] Fukuoka, T. and Takaki, T. (2004) Evaluations of the Tightening Process of Bolted Joint with Elastic Angle Control Method. *ASME/JSME* 2004 *Pressure Vessels and Piping Conference*, San Diego, 25-29 July 2004, 11-18. https://doi.org/10.1115/pvp2004-2617

[11] Gold, S., Gulber, A. and Pfitzer, A. (2020) Numerical Parameter Study of Stiffness of Bolt Connections. Project Work 01.07.2020, Technische Hochschule Ingolstadt,

Hochschule Landshut.

[12] Friedrich, C. and Thomala, W. (2000) Calculation of Tightening with Angular Control for Bolted Connections. *Materialwissenschaft und Werkstofftechnik*, **31**, 6-17.

[13] Chavan, D.K.L. and Tipnis, U. (2013) Study and Analysis of Angular Torquing of Engine Cylinder-Head Bolts Using Torque-to-Yield Bolts: A Case Study. *International Journal of Mechanical and Production Engineering Research and Development* (*IJMPERD*), **3**, 1-10.

[14] Toth, G.R. (2004) Torque and Angle Controlled Tightening over the Yield Point of a Screw—Based on Monte-Carlo Simulations. *Journal of Mechanical Design*, **126**, 729-736. https://doi.org/10.1115/1.1701877

[15] Xie, B.H., Fu, M.F. and Li, A.M. (2013) Theoretical Calculation and Experimental Study on Sung Torque and Angle for the Injector Clamp Tightening Bolt of Engine. *Applied Mechanics and Materials*, **351**, 1284-1288. https://doi.org/10.4028/www.scientific.net/amm.351-352.1284

[16] Santhosh, D.K., Suresh, K.S. and Solomon, C. (2017) Comparison of Torque and Torque-Angle Strategies for Tightening of High Strength Fasteners. *National Level PG Research Conference on Emerging Trends in Manufacturing*, Kerala, 9-10 June 2017. https://www.researchgate.net/publication/339439810_COMPARISON_OF_TORQUE_AND_TORQUE-ANGLE_STRATEGIES_FOR_TIGHTENING_OF_HIGH_STRENGTH_FASTENERS

[17] Eccles, B. (n.d.) A Case Study in Torque-Angle Tightening: Bolt Science. https://www.boltscience.com/pages/a-case-study-in-torque-angle-tightening.pdf

[18] Kraemer, F., Klein, M. and Oechsner, M. (2020) Fatigue Strength of Metric Steel Screws Depending on Pre-Load and Nut Type. *Engineering Failure Analysis*, **112**, Article ID: 104484. https://doi.org/10.1016/j.engfailanal.2020.104484

[19] ISO 16047 (2005) Fasteners—Torque/Clamp Force Testing.

[20] ISO 898-1 (2013) Mechanical Properties of Fasteners Made of Carbon Steel and Alloy Steel—Part 1: Bolts, Screws and Studs with Specified Property Classes—Coarse Thread and Fine Pitch Thread.

[21] ISO 6892-1 (2019) Metallic Materials—Tensile Testing—Part 1: Method of Test at Room Temperature.

[22] Fukuoka, T. and Takaki, T. (2003) Elastic Plastic Finite Element Analysis of Bolted Joint During Tightening Process. *Journal of Mechanical Design*, **125**, 823-830.

[23] Bickford, J.H. and Nassar, A.S. (1998) Handbook of Bolts and Bolted Joints. Marcel Dekker, Inc.

[24] Rasmussen, J., Norgaard, I.B., Haastrup, O. and Haastrup (1978) A Two Body Contact Problem with Friction. *Euromech Colloqium NR* 110 *Rimforsa*, 115-120.

Appendix

This appendix provides all comparative graphs "Clamp Force (N)/Angle (˚)" used to validate proposed model for all tested configurations.

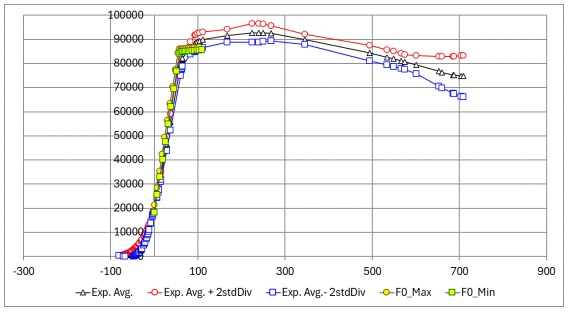

Conf 01-(HR-M12-L_k = 2d: μ_b = 0.07 ± 0.001; μ_t = 0.08 ± 0.006)

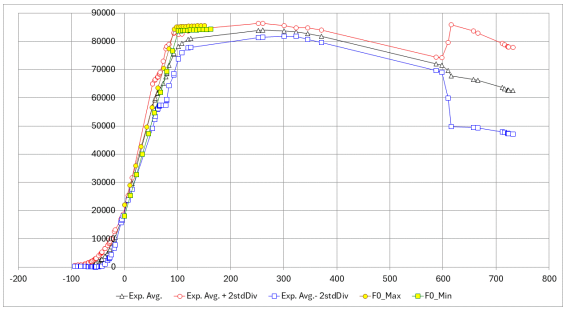

Conf 02-(HR-M12-L_k = 6d: μ_b = 0.08 ± 0.005; μ_t = 0.09 ± 0.008)

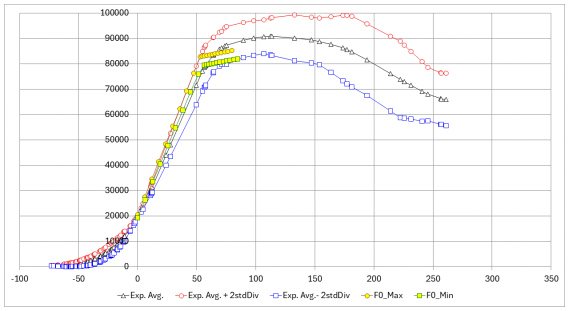

Conf 03-(HV-M12-L_k = 2d: μ_b = 0.10 ± 0.033; μ_t = 0.11 ± 0.018)

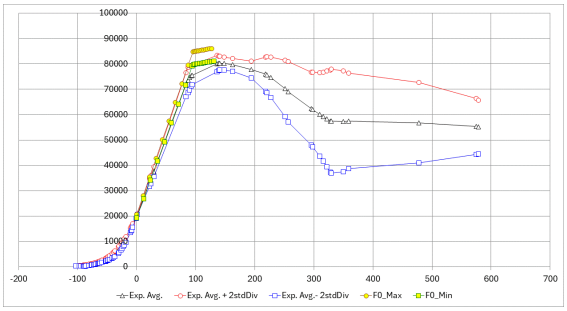

Conf 04-(HV-M12-L_k = 6d: μ_b = 0.08 ± 0.010; μ_t = 0.13 ± 0.024)

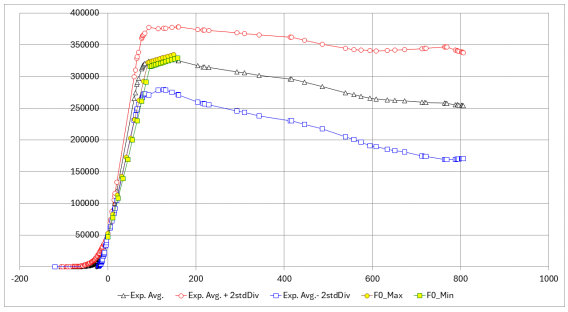

Conf 05-(HR-M24-L_k = 2d: μ_b = 0.07 ± 0.007; μ_t = 0.11 ± 0.009)

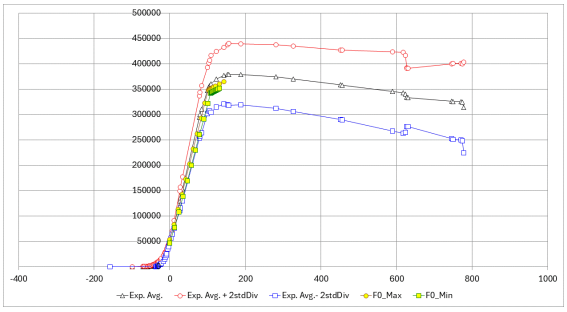

Conf 06-(HR-M24-L_k = 6d: μ_b = 0.07 ± 0.001; μ_t = 0.10 ± 0.005)

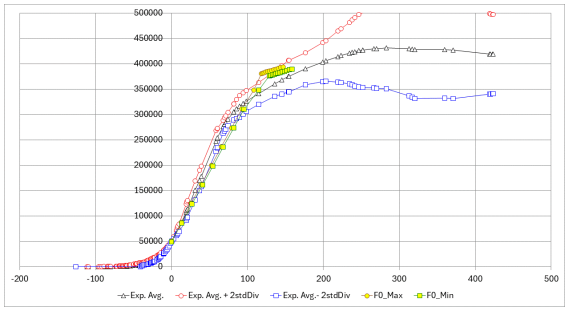

Conf 07-(HV-M24-L_k = 2d: μ_b = 0.08 ± 0.012; μ_t = 0.12 ± 0.005)

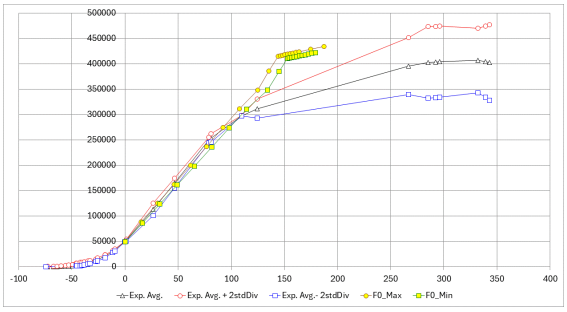

Conf 08-(HV-M24-L_k = 6d: μ_b = 0.07 ± 0.005; μ_t = 0.13 ± 0.013)

Continued

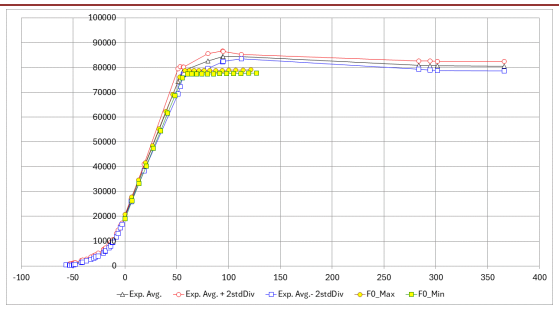

Conf 09-(H-M12-L_k = 2d: μ_b = 0.11 ± 0.013; μ_t = 0.14 ± 0.007)

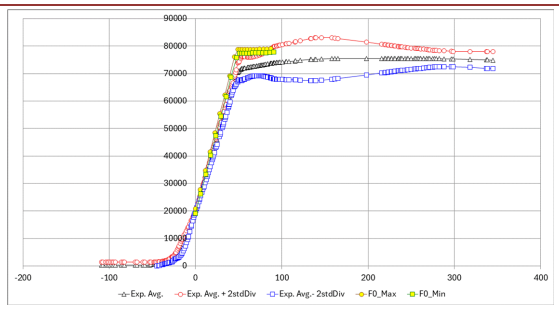

Conf 10-(H-M12-L_k = 1d: μ_b = 0.11 ± 0.013; μ_t = 0.14 ± 0.007)

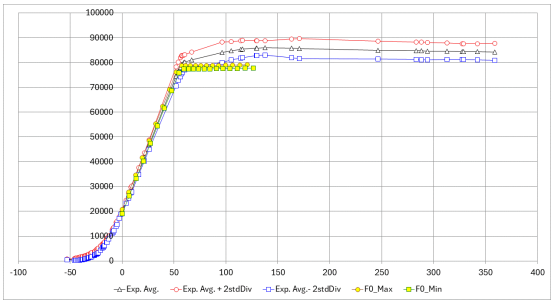

Conf 11-(H-M12-L_k = 2d: μ_b = 0.11 ± 0.013; μ_t = 0.14 ± 0.007)

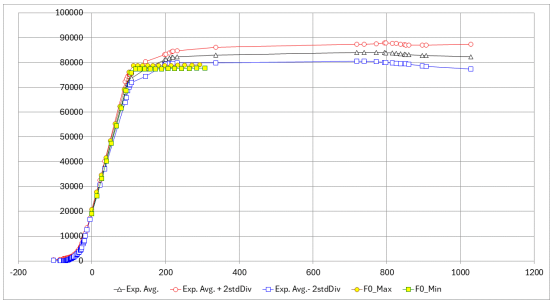

Conf 12-(H-M12-L_k = 6d: μ_b = 0.11 ± 0.013; μ_t = 0.14 ± 0.007)

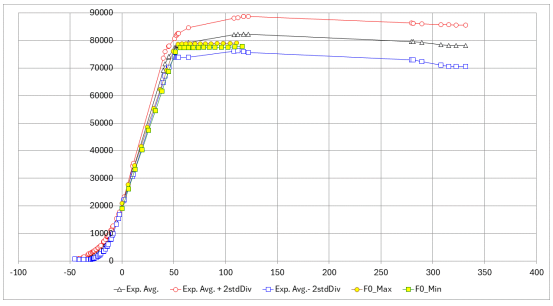

Conf 14-(H-M12-L_k = 2d: μ_b = 0.11 ± 0.013; μ_t = 0.14 ± 0.007)

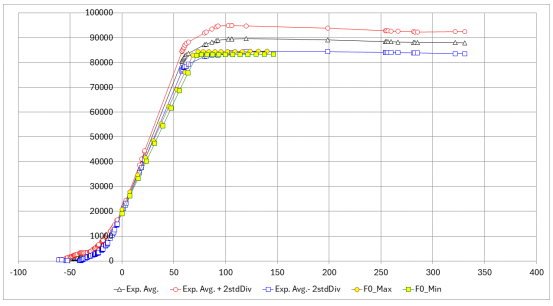

Conf 15-(H-M12-Lk = 2d: μ_b = 0.11 ± 0.013; μ_t = 0.08 ± 0.007)

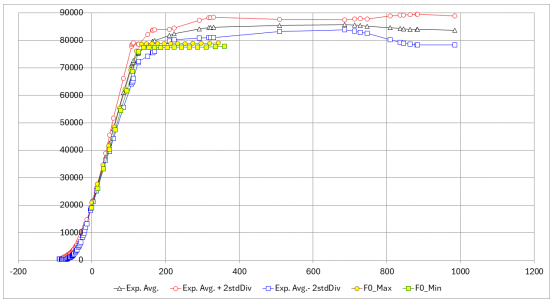

Conf 16-(H-M12-L_k = 6d: μ_b = 0.11 ± 0.013; μ_t = 0.14 ± 0.007)

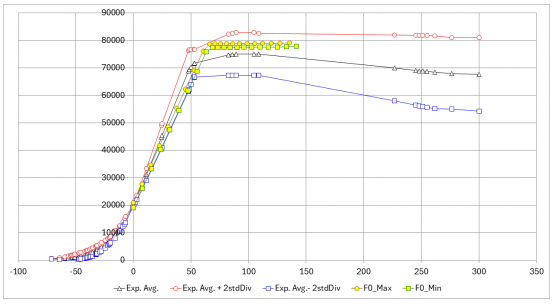

Conf 18-(H-M12-L_k = 2d: μ_b = 0.11 ± 0.013; μ_t = 0.14 ± 0.007)

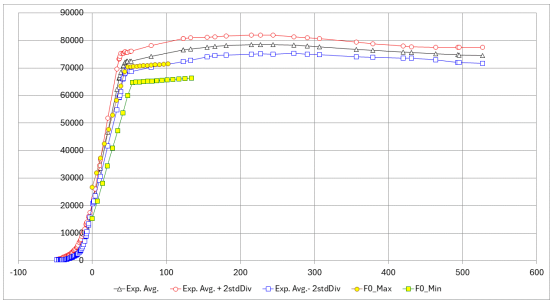

Conf 19-(Hex In-M12-L_k = 2d: μ_b = 0.15 ± 0.030; μ_t = 0.15 ± 0.03)

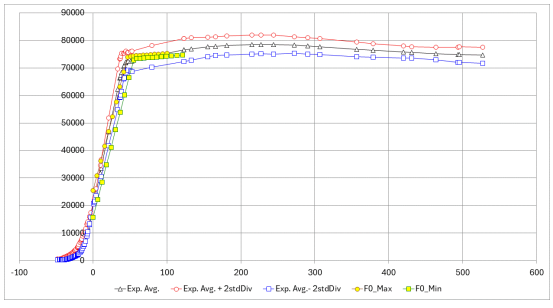

Conf 19-(Hex In-M12-L_k = 2d: μ_b = 0.11 ± 0.013; μ_t = 0.08 ± 0.006)

Continued

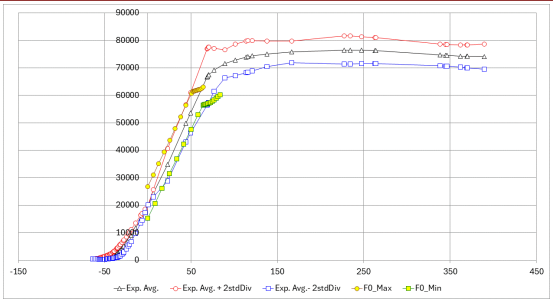

Conf 20-(Hex In-M12-L_k = 6d: $\mu_b = 0.15 \pm 0.030$; $\mu_t = 0.15 \pm 0.03$)

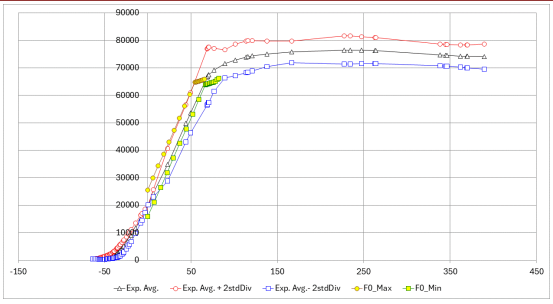

Conf 20-(H-M12-L_k = 6d: $\mu_b = 0.11 \pm 0.013$; $\mu_t = 0.08 \pm 0.006$)

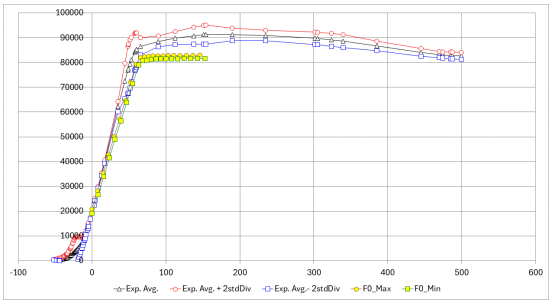

Conf 21-(Hex In-M12-L_k = 2d: $\mu_b = 0.12 \pm 0.013$; $\mu_t = 0.14 \pm 0.006$)

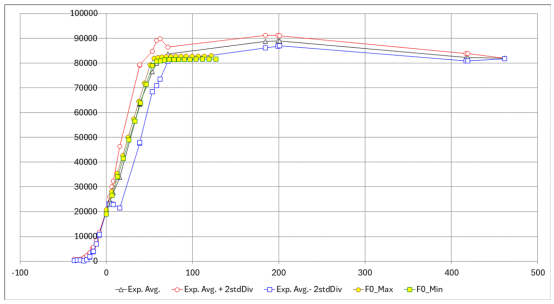

Conf 22-(Hex In-M12-L_k = 2d: $\mu_b = 0.12 \pm 0.013$; $\mu_t = 0.14 \pm 0.006$)

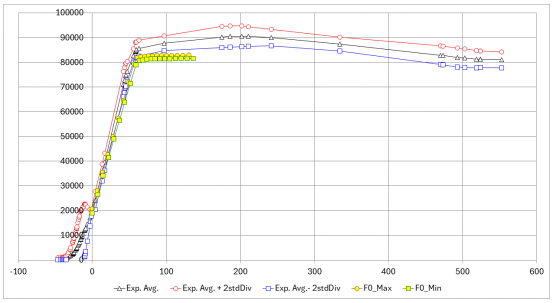

Conf 23-(Hex In-M12-L_k = 2d: $\mu_b = 0.12 \pm 0.013$; $\mu_t = 0.14 \pm 0.006$)

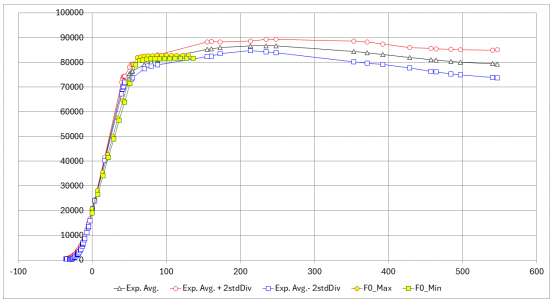

Conf 24-(Hex In-M12-L_k = 2d: $\mu_b = 0.12 \pm 0.013$; $\mu_t = 0.14 \pm 0.006$)

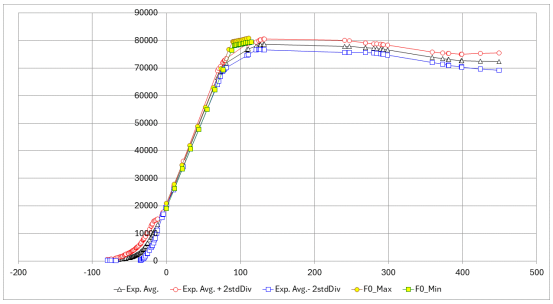

Conf 25-(Hex In-M12-L_k = 6d: $\mu_b = 0.12 \pm 0.015$; $\mu_t = 0.14 \pm 0.007$)

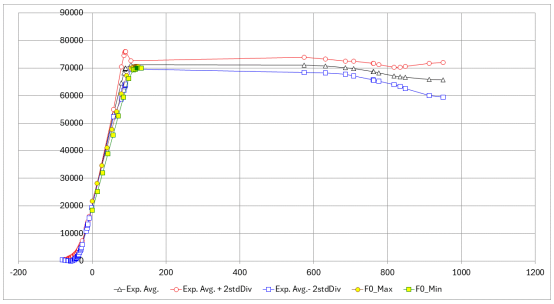

Conf 27-(H-M12-L_k = 6d: $\mu_b = 0.15 \pm 0.010$; $\mu_t = 0.14 \pm 0.004$)

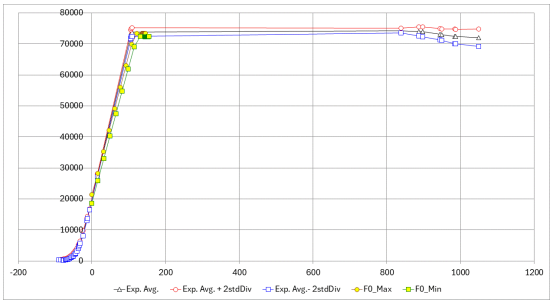

Conf 28-(H-M12-L_k = 6d: $\mu_b = 0.10 \pm 0.007$; $\mu_t = 0.13 \pm 0.005$)

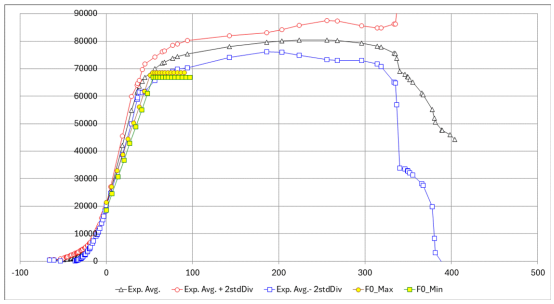

Conf 29-(Stud-M12-L_k = 2d: $\mu_b = 0.14 \pm 0.004$; $\mu_t = 0.15 \pm 0.011$)

Continued

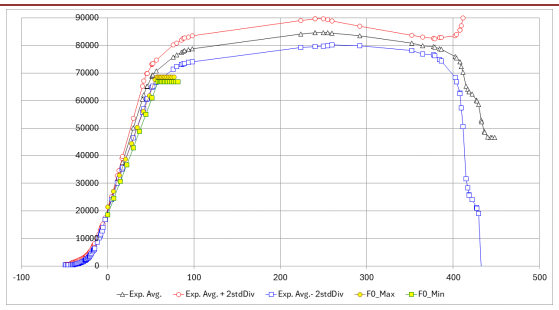

Conf 30A-(Stud-M12-L_k = 2d: $\mu_b = 0.16 \pm 0.005$; $\mu_t = 0.15 \pm 0.011$)

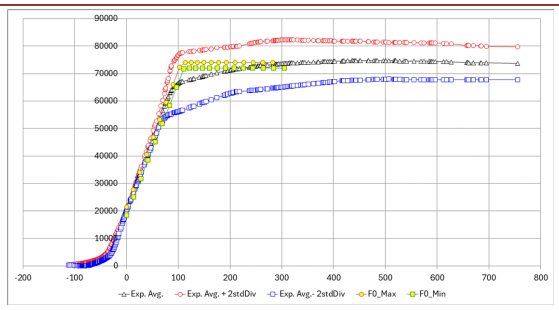

Conf 30B-(Stud-M12-L_k = 6d: $\mu_b = 0.15 \pm 0.006$; $\mu_t = 0.15 \pm 0.010$)

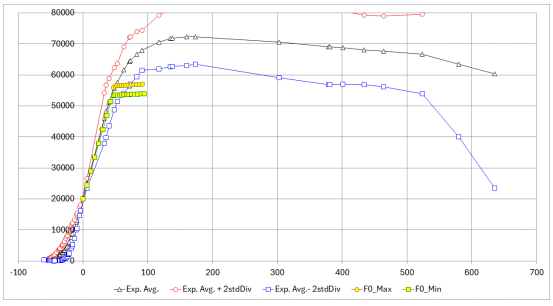

Conf 31-(H-M12-L_k = 2d: $\mu_b = 0.13 \pm 0.045$; $\mu_t = 0.16 \pm 0.020$)

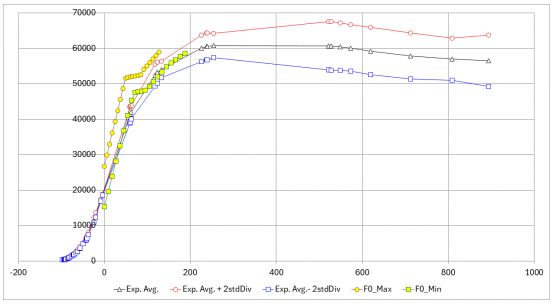

Conf 32-(H-M12-L_k = 6d: $\mu_b = 0.15 \pm 0.030$; $\mu_t = 0.15 \pm 0.030$)

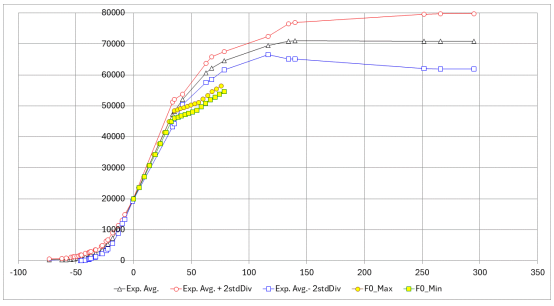

Conf 33-(H-M12-L_k = 2d: $\mu_b = 0.13 \pm 0.045$; $\mu_t = 0.16 \pm 0.020$)

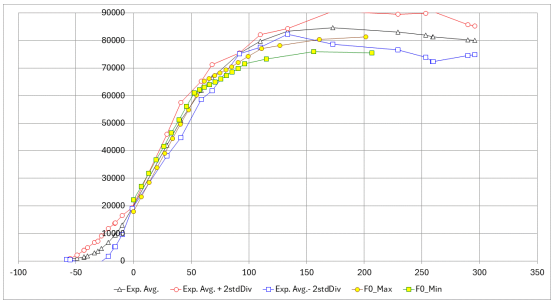

Conf 34-(H-M12-L_k = 2d: $\mu_b = 0.08 \pm 0.017$; $\mu_t = 0.11 \pm 0.025$)

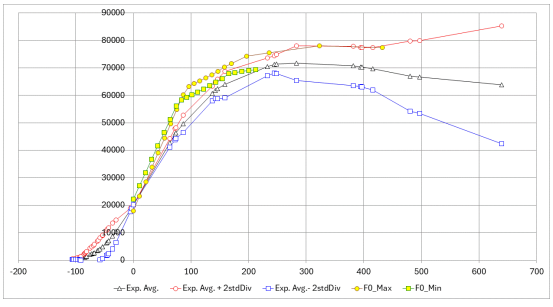

Conf 35-(H-M12-L_k = 6d: 0.15 ± 0.030; $\mu_t = 0.15 \pm 0.030$)

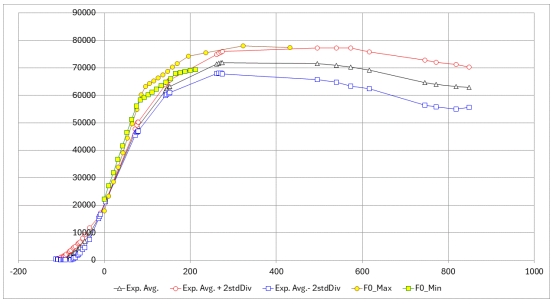

Conf 35B-(H-M12-L_k = 6d: 0.15 ± 0.030; $\mu_t = 0.15 \pm 0.030$)

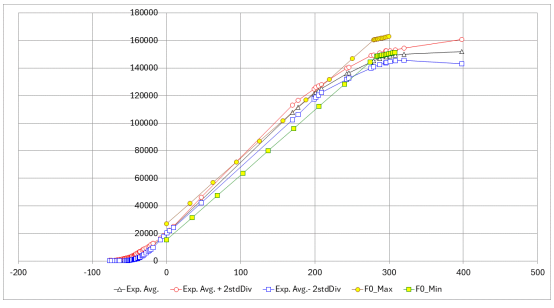

Conf 36-(BH-M12-Inconel-L_k = 6d: 0.15 ± 0.030; $\mu_t = 0.15 \pm 0.030$)

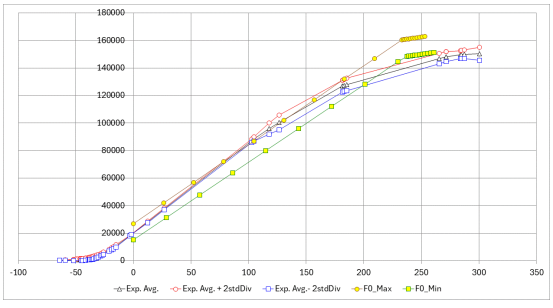

Conf 37-(BH-M12-Inconel-L_k = 6d: 0.15 ± 0.030; $\mu_t = 0.15 \pm 0.030$)